Vrije Universiteit Brussel

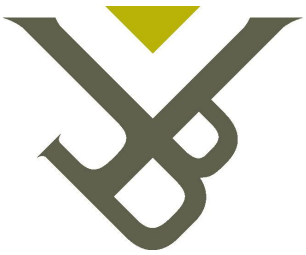

Faculteit Wetenschappen en Bio-ingenieurswetenschappen
Departement Natuurkunde

Study of the sensitivity of the IceCube-40 neutrino detector for neutralino dark matter annihilations in the Sun

Robbe Vansintjan

Promotor: Prof. Catherine De Clercq
Co-promotor Dr. Erik Strahler
Academiejaar: 2009 – 2010
Proefschrift ingediend met het oog op het behalen van de academische graad van master in de wetenschappen.

Acknowledgements

First and foremost I would like to thank all the people who helped me to make this thesis. My promotor Catherine De Clercq and co-promotor Erik Strahler for their guidance and the work they've done. Nick Van Eijndhoven for teaching me how to work with the IceCube software and always being willing to answer questions. My fellow students who shared my office Gerrit Van Onsem and Dennis Diederix for being such pleasant colleges and sharing their opinion on all the problems that came up. The entire IceCube group for all their input and creating such a pleasant work environment: Kael, Alberto, Debanjan, Mark, Alfio, Mathieu Kalpana, Daniel and Sabrina. Prof Ben Craps for commenting on the theoretical chapter of my thesis. The people in the computing support team for helping with all things related to computing. Marleen for helping with the paperwork.

I want to thank the Interuniversity Institude for High Energies (IIHE) for allawing me to perform this research.

Verder bedank ik graag mijn ouders, familie, vrienden en medestudenten over de jaren heen, voor hun steun en de fijne momenten die we samen hebben beleeft.

Contents

Chapter 1

Introduction

[1]

This thesis deals with the search for dark matter a hypothetical form of matter which was postulated to explain different kinds of cosmological phenomena. This dark matter is not described by the current standard model of particle physics.

The purpose of the thesis is to estimate the sensitivity of the IceCube detector for the indirect detection of dark matter during the year 2008 when 40 strings where deployed in the ice, about half of the total IceCube detector. First we will discuss the reasons for the postulation of dark matter, some of the properties it might have, possible dark matter candidates and the different type of dark matter detectors. Then we'll describe the IceCube neutrino detector and the different experimental goals the detector will try to reach. Finally will describe the experimental data and Monte Carlo data used and the analysis to distinguish the neutrino dark matter signal from the atmospheric background in the IceCube detector.

The physical quality that the IceCube neutrino telescopes measure directly is the neutrino-to-muon conversion rate $\Gamma_{\nu\to\mu}$. From this other relevant quantities like neutralino annihilation rates Γ_A and neutrino-induced muon fluxes ϕ_μ can be derived and compared to model predictions.

Chapter 2

Dark matter

2.1 Missing mass

A large part of the matter in the universe seems to be invisible to us. This dark matter or non-luminous matter was first noted by astrophysicist Fritz Zwicky in 1933[1, 2]. He estimated the mass of the Coma Cluster of galaxies in two ways by looking at the motions of galaxies near the edge of the cluster and by counting the number of galaxies and estimating the corresponding brightness of the cluster. He concluded that there was about 400 times more mass than was visually observable.

Some 40 years later Vera Rubin measured the orbital velocity of stars versus their distance from the centre of spiral galaxies[3]. In spiral galaxies most of the luminous matter is concentrated in the centre of the galaxy. Based on this we would expect that the radial velocity equals $v_{rad} = \sqrt{\frac{MG}{r}}$. What is measured is actually a flat velocity curve, as can be seen in figure 2.1. Rubin measured this for the Andromeda Nebula and by now this has been seen in many spiral galaxies. For large distances the rotation curve remains flat. This could be explained by a large amount of invisible matter in the halo of the galaxy.

Another important source of information regarding dark matter comes from gravitational lensing[1, 4]. Gravitational lensing is the bending of light around a massive object due to the warping of space-time predicted by general relativity. So if a massive object is between us (the observer) and a light source we can estimate its mass from the bending of the light sent out by the light source. This technique is used in galaxy clusters and with quasars as a light source. An advantage of this technique is that it does not rely on the dynamics of a system and so it is an independent way of measuring the mass. By measuring multiple objects with this technique, the total gravita-

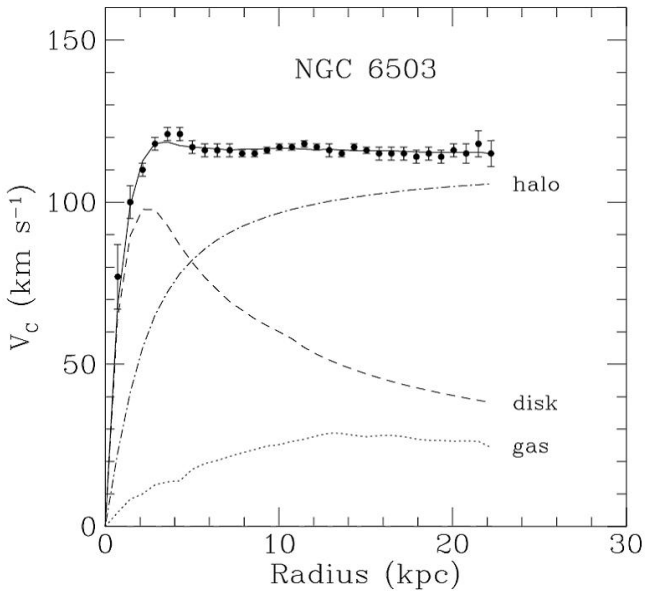

Figure 2.1: Rotation curve of NGC 6503. The dotted, dashed and dash-dotted lines are the expected contributions of gas, disk and dark matter, respectively. From Ref[14].

tional mass density of the universe can be estimated. The estimated mass density is $\rho_m = 2.2 \times 10^{-27}$ kg m^{-3} this is about 24% of the total energy density in the universe.[1, 6] Furthermore, using the gravitational lensing technique a map of the dark matter distribution in the universe has been made, as seen on figure 2.2. This map was made with data from the Hubble space telescope, from its largest survey of the universe, the Cosmic evolution survey. The survey looks at an area of the sky 9 times that of the moon and stretches halfway back to the beginning of the universe. It shows how dark matter is distributed across the universe, how it clumps together under the pull of gravity and how baryonic matter, mostly in the form of galaxies, accumulates in the densest concentrations of dark matter.[5]

Dark matter is also an important component in the Big Bang model of cosmology, used to explain the large structure formation in the universe. In the current standard model of cosmology, or ΛCDM model, dark matter is a parameter in the Friedman equations[1, 6]. These equations describe the expansion of space in an isotropic and homogenous model of the universe, an assumption that seems reasonable in view of the observation of the uniformity of the cosmic background radiation over large distances, of about a 100Mpc. These assumptions imply a specific form of the space-time metric which can

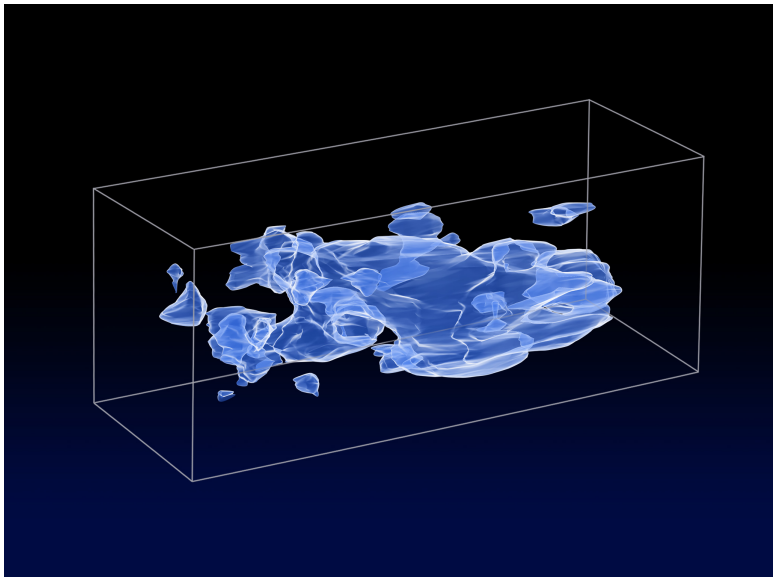

Figure 2.2: The distribution of mass in the Hubble Space Telescope COSMOS survey, determined from measurements of weak gravitational lensing. The field of view covers about nine times the size of the full moon, and the third dimension stretches from redshift z = 0 to z = 1. The figure shows one isosurface of the gravitational potential.[7]

be expressed as the Robertson-Walker metric

$$ds^2 = -c^2dt^2 + a^2(t)\left[\frac{dr^2}{1-kr^2} + r^2d\Omega^2\right] \tag{2.1}$$

where $a(t)$ is the scale factor and k is a constant describing the curvature of space. With this metric the Einstein equations can be solved to get the two independent Friedman equations.

$$H^2 = \left(\frac{\dot{a}}{a}\right)^2 = \frac{8\pi G}{3}\rho - \frac{kc^2}{a^2} + \frac{\Lambda c^2}{3} \tag{2.2}$$

$$\frac{\ddot{a}}{a} = -\frac{4\pi G}{3}\left(\rho + \frac{3p}{c^2}\right) + \frac{\Lambda c^2}{3} \tag{2.3}$$

The first Friedman equation describes the expansion rate and the second one describes the change in expansion rate.

Furthermore, observation suggests that structure formation proceeds hierarchically, with the smallest structures like stars collapsing first followed by the forming of galaxies and then clusters of galaxies. Ordinary baryonic

matter would heat up too much during the collapse due to gravitational contraction. So dark matter is needed to act as a compactor. This model is in agreement with surveys of the visible structure of the universe and the dark matter necessary to explain the structure formation corresponds precisely to the dark matter predictions of the cosmic microwave background. These observations even tell us something about the nature of dark matter; namely that it consists for the most part of non-relativistic, or cold dark matter. This suggests relatively massive particles, because these particles would be non-relativistic when they freeze-out(When the universe expands temperature and particle density drop this will cause particles to fall out of thermal equilibrium, the moment this happens it is said that they freeze-out. It is assumed that most of the dark matter was produced during the Big Bang).[9]

Dark matter is also used in models describing spiral galaxies. In models without a dark halo it turns out that the structure of a spiral galaxy is not preserved over many rotations. This is in contradiction with the fact that spiral galaxies appear stable. [10, 11]

Finally, the measurements of the cosmic microwave background allow us to make a prediction of the matter and energy present in the universe. About 4.6% of the universe is made up of ordinary baryonic matter, 23% is made up out of dark matter and 72% is thought to consist of dark energy, a component we know even less about. It should be noted that of the total baryonic matter deduced from primordial nucleosynthesis, only 10% is accounted for in the luminous matter in stars. Hot gas in galaxy clusters is a further 40%. This leaves half the baryonic matter unaccounted for. This missing baryonic matter could be located in dark, compact stellar objects (MACHOs or massive astrophysical compact halo objects, discussed later) or this missing baryonic matter could be associated with blazers(an active galactic nuclus which emits photons in the TeV range).[1]

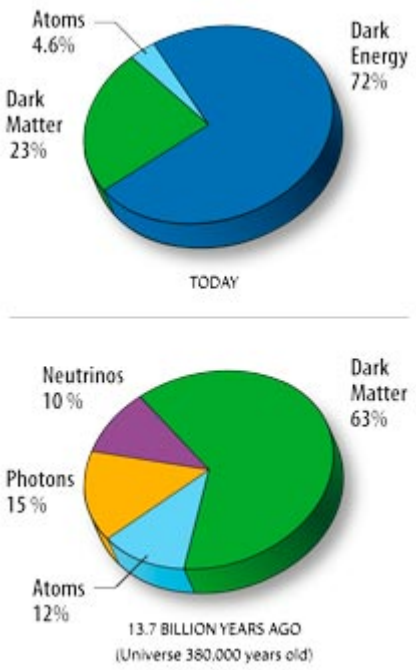

Figure 2.3: The Content of the universe in a pie chart[8]

2.2 Dark matter candidates

Now that we have discussed the reason to assume the existence of dark matter, we'll have a look at the possible candidates. The first possibility is that there simply is no dark matter at all and that the observations can be explained by an adaptation of the laws of gravity on a larger scale, for instance alternative theories like MOND (modified Newtonian dynamics)[12]. These theories have become less credible after the observation of several colliding galaxies in which the distribution of matter has been determined through the observation of visible light from the stars, x-rays from the gas and gravitational matter through gravitational lensing. In figure 2.4 the visible and x-rays are shown in red and the dark matter measured with gravitational lenzing is shown in blue.

What happened in these galaxies (fig. 2.4) is that the electromagnetic interacting matter interacted more with each other in passing and so slowed down more than the dark matter, causing a separation in the different types of matter. From the fact that the dark matter components pass through each other so easily one can derive a constraint on the self-interaction cross

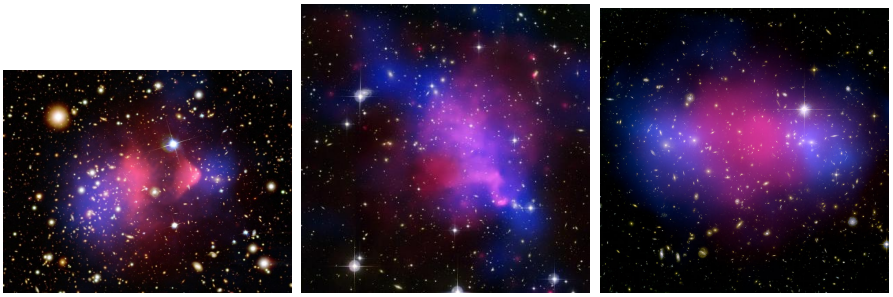

Figure 2.4: Three colliding galaxies where the visible matter and the dark matter have separated. From left to right; The Bullet Cluster, Rrainwreck and Baby Bullet. The X-rays and visible light are shown in red and the dark matter measured with gravitational lenzing is shown in blue[7].

section of dark matter[13].

$$\sigma/M \leq 1.25 cm^2/g$$

The first dark matter candidates we'll discuss are those described in the present standard model of particle physics or composed of standard model particles; MACHOs and neutrinos.

MACHOs (Massive Astrophysical Compact Halo Objects) are astronomical object composed of baryonic matter that emit no or very little radiation, like black holes, neutron stars, brown dwarfs, exoplanets, etc. Because MACHOs emit no light they are very hard to detect. They have been searched for using weak gravitational lensing techniques by different groups. The result of these searches and observations of the Hubble telescope show that MACHOs account for only a small fraction of all the non-luminous baryonic matter in our own galaxy and make a neglectible contribution to the dark matter in the universe.[14]

Now we look at different kinds of individual particles like neutrinos. The particle candidates can be divided in three types. These three types of matter are hot dark matter which are particles that are ultra relativistic, warm dark matter which are particles that are relativistic and cold dark matter which are particles that are non-relativistic.

Through the observation of the cosmic background radiation and structure formation, we know that the majority of the dark matter consists of cold dark matter, because relativistic particles like photons iron out primordial density fluctuations(which are studied through observations of the anisotropies in the microwave background and large scale structure formation). The fraction of dark matter which could be hot is of the order of 30%

or less.[1, 14]

Neutrinos were once a popular dark matter candidate. They have an appealing quality as a dark matter candidate because unlike other candidates we know that neutrinos exist. Like photons, neutrinos would have been produced in great amounts during the early stages of the universe. The relic microwave neutrino number density would be comparable with the relic photon number density.

$$N_\nu = \left(\frac{3}{11}\right) N_\gamma = 113 cm^{-3}$$

In order for the neutrino energy density to be equal to the critical energy density of dark matter the sum of the masses of the three flavours must have the value.

$$\sum m_\nu c^2 = 47 eV$$

This is much higher than the upper limits on neutrino masses determined in laboratory experiments. Furthermore, because of its low mass the neutrino would be relativistic. As mentioned before, cosmological observations show that dark matter is mostly non relativistic. Therefore, standard model neutrinos can't be a major contributor to dark matter.[1, 14]

Now we consider particles that have not been seen yet. These particles originate in extensions of the standard model of particle physics. One such dark matter candidate is the axion. This particle was postulated to explain the absence of CP violation in the strong interactions[15]. The axion decays into two photons. If the particle would have a sufficiently small mass it would have a long lifetime and survive as a relic of the Big Bang. Strong limits on the axion mass have been determened through observations of the cooling rate of red giant stars.[1, 16]

$$m_a < 0.01 eV/c^2$$

The smallness of the axion mass would eliminate axions as a dark matter candidate using the same argument as for the neutrinos. However axions couple very weakly and would never have been in thermal equilibrium with other particles in the early stages of the universe. In order to account for all dark matter, axions should have a mass of at least $10^{-5} - 10^{-3}$ eV.[1, 14]

The most popular candidates at the moment are Weakly Interacting Massive Particles (WIMPs). A particle with a high mass would have a non relativistic speed and a particle that interacts weakly gives us a chance to detect

it. It would be exceedingly difficult to detect particles that only interact gravitationally.

For several reasons supersymmetric (SUSY)[14] particles are the most popular particle to be a WIMP. Supersymmetry is an extension of the current standard model of particle physics. It is a symmetry between fermions (particles with spin $n\bar{h}/2$) and bosons (particles with a spin $n\bar{h}$). For every fermion a new type of boson would exist with the same quantum numbers and vice versa, with the exeption of spin. Supersymmetry solves two problems with the current standard model of particle physics. One of the problems is that the Higgs mass is unstable for higher order loop radiative corrections. This is known as the hierarchy problem. The second problem is the unsuccessful unification of the electroweak and the strong force at higher energies. Both are solved by introducing SUSY. [1]

If supersymmetry existed at low energies we would have detected these particles already, so we assume that supersymmetry exists at higher energies and is broken at lower energies. This breaking adds more than a hundred free parameters to the 19 standard model parameters. This is very impractical to work with but SUSY models can be simplified by making a couple of assumptions, depending on the model. For example the existence of two Higgs doublets to which spin 1/2 higgsinos are associated. Also R-parity is assumed to explain the stability of the proton. These models are called minimal supersymmetry (MSSM). Most MSSM models predict the neutralino as the lightest supersymmetric particle.

The neutralino is a majorana fermion and a linear combination of the mass eigenstates of the Bino, the Wino (The superpartners of $\widetilde{B}$ and $\widetilde{W}_3$) and two higgsinos. These particles have the same quantum numbers.

$$\widetilde{\chi}_i^0 = N_{i1}\widetilde{B} + N_{i2}\widetilde{W}^3 + N_{i3}\widetilde{H}_1^0 + N_{i4}\widetilde{H}_2^0$$

The neutralino would be stable in theories with conservation of R-parity. Because it is a majorana particle it would be its own anti-particle. Therefore, it will annihilate in pairs.[17]

If WIMPs exist they should occasionally interact with ordinary matter. This happens in two ways; by spin-independent (e.g. Higgs exchange) and by spin-dependent (e.g. Z-boson exchange) interactions.[18] WIMPs that pass through objects with a large mass and volume like the Sun would lose kinetic energy through these interactions. If their energy is low enough they would become trapped in the gravitational field of the Sun. Through interactions with the baryonic matter the WIMP will continue to lose energy, decreasing its orbit around the Sun, and eventually accumulating in its centre. If the WIMPs are neutralinos they will annihilate in pairs into the lighter standard

model particles. The WIMPs in the Sun build up over its lifetime until an equilibrium is reached between the capture and the annihilation rates. In equilibrium the annihilation rate is half the capture rate because of the pair wise annihilation. The WIMPs in the Sun have built up during its lifetime. So the Sun has been accumulating dark matter throughout the galaxy. Therefore, different kind of dark halo structures have been averaged out. So for a give WIMP model the signal in the detector can be exactly determent The solar capture rate of WIMPs is given by

$$\begin{aligned} C^{\odot} \approx 1.3 \times 10^{21} sec^{-1} \left(\frac{\rho_{local}}{0.3 GeV/cm^3} \right) \left(\frac{270 km/s}{v_{local}} \right) \\ \times \left(\frac{100 GeV}{m_{\chi}} \right) \times \sum \left(\frac{A_i (\sigma_{\chi i,SD} + \sigma_{\chi i,SI}) S(\frac{m_{\chi}}{m_i})}{10^{-6} pb} \right) \end{aligned} \tag{2.4}$$

where ρ_{local} is the local dark matter density and v_{local} is the local rms velocity of halo dark matter particles. $\sigma_{\chi i,SD}$ and $\sigma_{\chi i,SI}$ are the spin-dependent and spin-independent elastic scattering cross sections of the WIMP with nuclei species i, and A_i is a factor denoting the relative abundance and form factor for each species. The function S is given by

$$S(x) = \left[\frac{A(x)^{3/2}}{1 + A(x)^{3/2}} \right]^{2/3} \tag{2.5}$$

where

$$A(x) = \frac{3}{2} \frac{x}{(x-1)^2} \left(\frac{v_{esc}}{v_{local}} \right)^2 \tag{2.6}$$

If we neglect the WIMP evaporation rate and assume a constant capture, the WIMP annihilation rate is given by

$$\Gamma = \frac{1}{2} C^{\odot} \tanh^2 \left(\sqrt{C^{\odot} A^{\odot}} t_{\odot} \right) \tag{2.7}$$

For typical neutralino models, equilibrium in the Sun is already reached 10^8 years after its birth. In equilibrium, the annihilation rate is directly proportional to the capture rate and, hence, the total elastic neutralino-nucleon cross section

Neutralinos have many different annihilation channels. Of all the known particles that remain after annihilation and decay the neutrino is the only particle that can reach the Earth where it hopefully will be detected in one of the neutrino detectors. Because the energy of the neutrinos depends on the annihilation channel of the neutralino and there are many different channels,

we look at the extremes of the energy distribution. The soft channel or the $b\bar{b}$ channel gives a lower neutrino energy distribution

$$\tilde{\chi}_0 + \tilde{\chi}_0 \longrightarrow b\bar{b}$$

and the hard channel or the W^+W^- channel gives a higher energy distribution.

$$\tilde{\chi}_0 + \tilde{\chi}_0 \longrightarrow W^+ + W^-$$

In figure 2.5 we show the energy spectrum for both these annihilation channels.

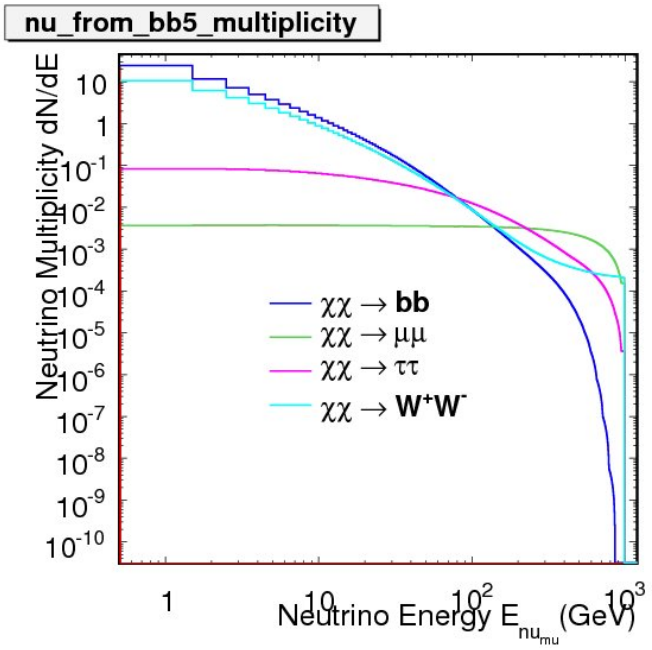

Figure 2.5: The neutralino energy spectrum for different annihilation channels.

2.3 Types of experiments

If dark matter is made up of WIMPs then a large number of them must pass through the Earth and the Sun. There are many experiments aiming to test this by searching for a WIMP signal. These experiments can be divided into three classes: direct detection experiments, indirect detection experiments and collider experiments.[1, 14]

2.3.1 Direct detection experiments

Direct detection experiments are placed deep underground to reduce the background from cosmic rays. This still leaves background from radioactive materials, neutrinos and photons. Most of the experiments use one of two detection techniques. Cryogenic detectors (e.g. CDMS[19]) operate at temperatures below 100 mK and measure the recoil energy of a WIMP particle scattering on an atom in a lattice. A phonon and an electron signal are measured to distinguish the dark matter signal from background. Noble liquid detectors (e.g. XENON100 [20]) measure the collision of a particle on the atoms in a noble liquid. These collisions produce a flash of scintillation light which is measured together with phonons.

2.3.2 Indirect detection experiments

If WIMPs are majorama particles then two colliding WIMPs would annihilate into standard model articles. WIMPs would also lose kinetic energy due to weak interactions with ordinary matter. In this way they would accumulate in the centre of heavy objects like the Sun and the Earth. A neutrino or anti-neutrino signal coming from these sources would be a strong, indirect, indication for WIMPs as dark matter detectors like IceCube (the subject of this thesis) and ANTARES[22] are currently looking for these signals. Furthermore, gamma ray signals from dense regions of the galactic halo, such as the galactic center and the detection of cosmic positrons and anti-protons can be valuable tools in searching for particle dark matter. For neutralino dark matter the sensitivity of direct detection experiments to the spin independent cross section increases with the square of the atomic number of the detector material. With the improvements in direct detection methods the indirect neutralino dark matter searches become less competitive for spin independent cross sections but remain competitive for spin dependent cross sections.

2.3.3 Collider experiments

Collider experiments like the LHC[23] could produce dark matter. This matter will not be detected in the LHC detectors but could be seen in the form of missing energy and momentum. But even if the LHC would measure this missing energy, direct detection is still necessary to prove the existence of the dark matter particle and to determine its properties. However the detectors

at the LHC could detect charged SUSY particles. If this happens it would be a good indication for the neutralino as a dark matter candidate.

Currently there is one experiment that claims to have detected dark matter namely, DAMA/LIBRA[21]. The experiment used a thallium-doped sodium iodide (NaI) scintillator and measured the annual dark matter fluctuation caused by the revolution of the Earth around the Sun. The results of this experiment are controversial because other searches have not detected nuclear recoils due to dark matter interactions. All these other searches use sophisticated background elimination techniques instead of the annual modulation technique. An independent check of the DAMA/LIBRA signal using the Super-Kamiokande neutrino detector is proposed.[25]

The CDMSII collaboration which uses germanium and silicon crystal detectors announced the possible detection of two candidats events which could be WIMPs but have a 23% chance of being background.[24]

Chapter 3

Neutrino Interactions and the IceCube Detector

IceCube is a neutrino telescope currently under construction at the South Pole and scheduled to be completed in 2011. Similar to its predecessor AMANDA, IceCube looks at neutrinos through the measurement of Cherenkov light. The detector is made up of optical sensors called Digital Optical Modules (DOMs), each with a photomultiplier tube (PMT) and a data acquisition computer. These DOMs are attached to strings which are lowered into the Antarctic ice at depths between 1450 meters to 2450 meters. IceCube is designed to look for point sources of neutrinos in the TeV -PeV energy range to explore the highest-energy astrophysical processes. With the inclusion of Deepcore in the IceCube string array the observable energies will go below 100 GeV.[26]

3.1 Neutrinos and their interaction with matter

Neutrinos interact rarely with ordinary matter and when they do it's mainly through the weak force (assuming they have mass they should also interact gravitationally). In this way a neutrino can interact with a nucleus in two different ways; through the exchange of a neutral Z boson known as the neutral current or through the exchange of W^+ or W^- boson known as the charged current. The neutral current will only scatter the neutrino from the nucleus and leave the neutrino unaltered while the charged current will change the neutrino into a charged lepton:

$$\nu_l(\bar{\nu}_l) + N \rightarrow l^-(l^+) + X$$

More precisely the neutrino will be annihilated and a lepton will be created,which lepton depends on the flavour of the neutrino.

The cross section for the charged current interaction is higher than that of the neutral current interaction. Also the cross section of the anti-neutrinos is lower than that of the neutrinos. The neutrinos interact only with the valence down quarks in the nucleus and the anti-neutrinos interact only with the valance up quarks in the nucleon. [27]

The mean angle between the muon-neutrino and the muon paths can be approximated with the formula.

$$\langle \theta_{\nu\mu} \rangle \approx \frac{0,7^\circ}{(E_\nu / TeV)^{0,7}} \tag{3.1}$$

The average angle is less than 1° above 0,6 TeV. Because of the small angle we have a good resolution on the neutrino direction at high energies. For lower energy this imposes a limit on the precision of the direction of the neutrino.[28]

When a neutrino interacts with a nucleus through the charged current it results in the creation of an electron, muon or tau. When an electron is produced in an interaction it will result produce electromagnetic shower of a couple of meters, due to its low mass. These showers are too short to be effectively measured for track reconstruction(see fig. 3.1). The tau lepton is the most massive lepton of the three and therefore decays the fastest. It has a lifetime of $(290.6 \pm 1,0) \times 10^{-15}$ seconds. So when a tau is created in the ice it quickly decays into leptons and hadrons. A fraction of these decays (17.7 %) result in muons.[31] If the energy of the tau neutrino is high enough the creation of a tau and its decay will produce two distinct particle showers. This is called a double bang event. Currently studies are being done to effectively measure and reconstruct these events.

Of all three leptons the muons travel the farthest. When the muon travels through the ice at a speed greater than the speed of light in the ice it will emit Cherenkov light(see fig. 3.1). Cherenkov light is caused by the disturbance of the electromagnetic field of the medium when a charged particle like a muon passes. The atoms in the medium become polerized. When the electrons restore themselves to equilibrium they will emit photons. The photons will interfere constructively if the passing particle moves faster than the speed of light.

This requirement for constructive interference tells us that there is a minimum energy that the muons must have in order to be detected.

$$E_{muon}(\lambda) = \frac{m_{muon}}{\sqrt{1 - \left(\frac{1}{n(\lambda)}\right)^2}} \tag{3.2}$$

For ice the minimum energy is a 160 MeV.

The Cherenkov light will be emitted around the particle track in a cone, as shown in fig. 3.1. The size of the cone depends on the index of refraction of the material n and on the speed of the particle divided by the speed of light in vacuüm $\beta = \frac{v}{c}$.

$$cos(\beta_{cone}) = \frac{1}{n\beta} \tag{3.3}$$

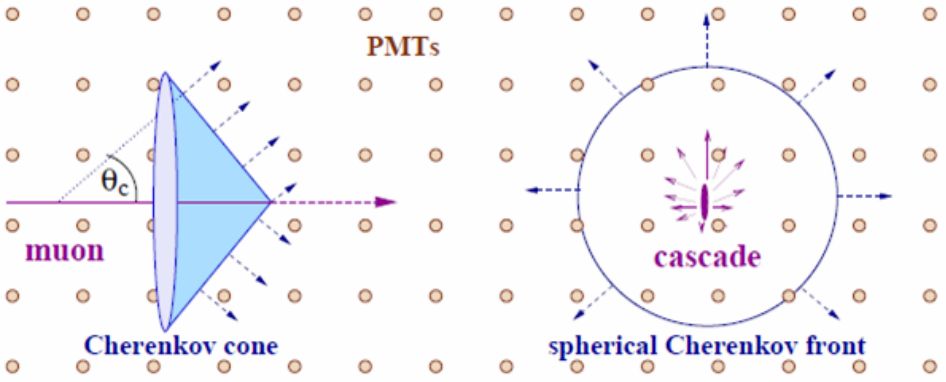

Figure 3.1: The figure on the left shows a Cherenkov cone produced by a muon. The right picture shows the cherenkov light produced by an electron or a tau particle during creation or decay.[45]

If we assume that $\beta = 1$ and $n_{ice} = 1.33$ we find a Cherenkov angle of $41,2°$. [29] The number of Cherenkov photons emitted per unit path length can be calculated with the formula

$$\frac{dN}{dx} = 2\pi\alpha \int (1 - \frac{1}{n^2\beta^2})\frac{d\lambda}{\lambda^2} \tag{3.4}$$

where α is the fine structure constant and λ is the wavelength of the emitted photon. Normally about 260 Cherenkov photons are emitted per centimetre in the visible spectrum.[30] In a transparent medium like ice the emitted photons can travel distances of a few hundred meters. These photons can be detected with DOMs. Through these measurements we can reconstruct the track of the muon, which we'll dicuss later on.

The energy loss of muons below 1TeV is dominated by four processes; ionization, pair-production, brehmsstrahlung and photo-nuclear interaction. During these processes light is emitted which can also be detected. This light becomes more important for higher energy neutrinos. The mean distance a muon will move through the ice before stopping can be approximated from

a parameterization of the energy loss with the formula.

$$R_\mu \approx \frac{1}{b} ln \left(\frac{E_\mu}{E_c} - 1 \right) \tag{3.5}$$

where $b = 3 \times 10^{-4} m^{-1}$ and $E_c = 650 GeV$. A 100/1000/10000 GeV muon travels on average roughly 477/3105/9321 m of ice.[18]

In this analysis muon events will be used. In a transparent medium like ice the light created by the muon will travel great distances. However, when it travels through the ice the light will be absorbed and scattered, as seen in fig. 3.2. You could divide this absorption and scattering in two types; intrinsicly caused by the medium itself and absorption and scattering caused by impurities inside the ice. An electromagnetic wave passing through a medium will interact in two ways with the atoms and molecules inside the material. When a photon interacts with the valence electrons, in the material depending on the energy of the photon the electron will either go into an excited state or not. An isolated atom or molecule will emit a photon again with the same energy in a random direction. In a dense material this is different. If a valence electron goes into an excited state it will go back into a relaxed state by emitting its energy as heat. So there are intrinsic absorption bands in the material. For ice this is at the edges of the visible spectrum as seen on figure 3.2. A second difference is that while atoms emit photons in all directions the emitted electromagnetic wave interferes only constructively in one direction. So light will scatter in the material if the atoms are missing in the lattice or when the density of the material changes. Two important causes of absorption and scattering are dust in the ice and air bubbles. The air bubbles are mostly a problem in the top layers of the ice since they disappear because of pressure exerted on them. In the deeper layers they would have been under pressure for a longer period of time. Below 1300 m most have disappeared. They can still be a problem where the holes have been drilled to lower the IceCube strings.

The dust forms a problem depending on the depth in ice. Sevral ice layers were created during different geological periods of the Earth with different volcanic activity. There is a very thick dust layer between 2000 m and 2100 m depth.[32]

All these things have to be taken into account during the reconstruction of the track and the simulation of the detector response.

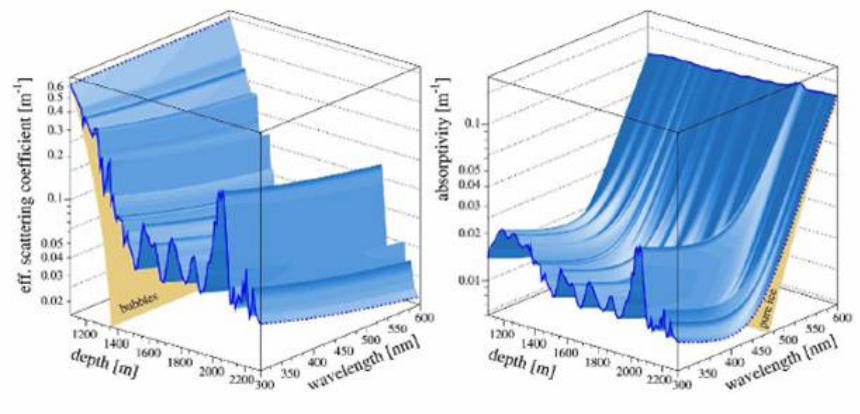

Figure 3.2: Effective scattering coefficient (left) and absorptivity (right) for deep South Pole ice as a function of wavelength and depth. Effective scattering coefficient is the inverse of the effective scattering length and absorptivity is the inverse of the absorption length[32].

3.2 IceCube: a Cherenkov neutrino detector

The IceCube detector is an array of Digital Optical Modules (DOMs) placed on strings and put in the Antarctic ice. The detector can be divided into three parts. The first part is InIce which is the main detector array. The second Deepcore is a denser array of DOMs placed at the centre of the detector and in the clearer parts of the ice. The third part is IceTop an array of Cherenkov detector, used for cosmic ray measurements, placed on the surface of the ice.

The detection principle was explained in more detail above. In short, a neutrino interacts in the ice through the charged current whereby it changes into a charged lepton. If that lepton is a muon the particle will travel a relatively large distance through the ice. Along its trajectory the muon will emit Cherenkov light, which will be detected by the DOMs inside the ice. From the measurement of the emitted light we reconstruct the track of the muon and the neutrino direction.

3.2.1 Detector components.

The IceCube observatory consists of 3 parts(see fig. 3.3, 3.4)[26]. The biggest part is InIce. This is the main detector array consisting of 80 strings with each string containing 60 DOMs. It's placed at a depth ranging from 1.450 to 2.450 meters, into holes melted in the ice using a hot water drill.

The second part Deep Core. Is a low energy extension of IceCube. It is

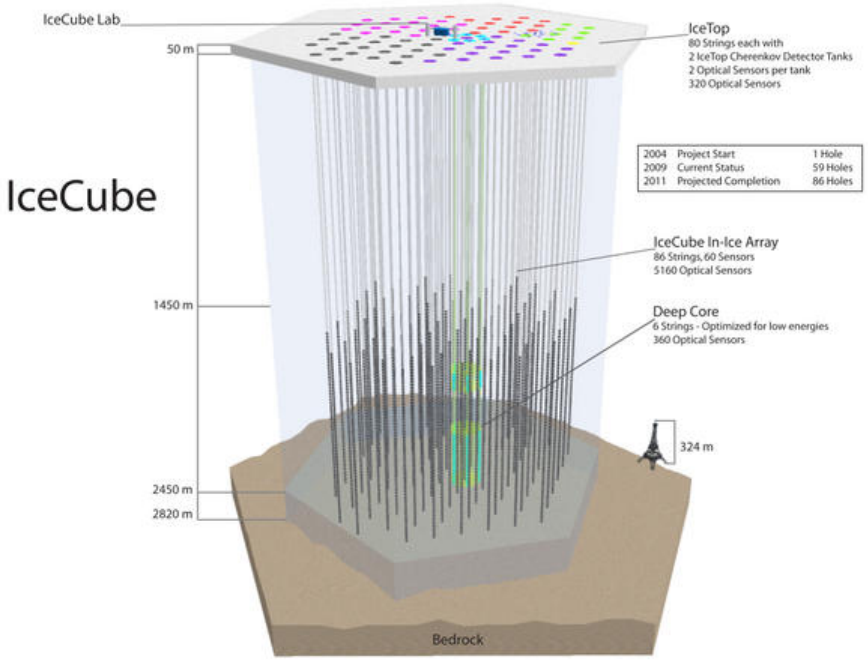

Figure 3.3: The IceCube detector.

denser array of 360 Cherenkov detectors placed at the centre of IceCube in the clear ice between 1850 m and 2107 m depth. With Deepcore the lower energy neutrinos will be observable as well as the southern hemisphere, using InIce as a veto.

The third part IceTop. At the surface above each string two icetanks with 2 DOMs are installed. The main goal of IceTop is the measurement of the spectrum and the chemical composition of high-energy cosmic rays through the air shower measurement technique. IceTop can also be used as a veto against cosmic rays in IceCube. A muon that was measured first in IceTop wasn't created in the ice through neutrino interactions.

3.2.2 The IceCube array

The data used in this thesis was taken when 40 strings were in the ice. Figure 3.4 shows the deployment of strings for different seasons. The 40 string array was completed during the season of 2007-2008 and the IceCubr-40 data taking ran from April 08 to March 09. From the figure we can see that the 40 string IceCube detector is asymmetric. High energy neutrinos coming from the Sun enter the detector roughly horizontally through the side, becouse of the

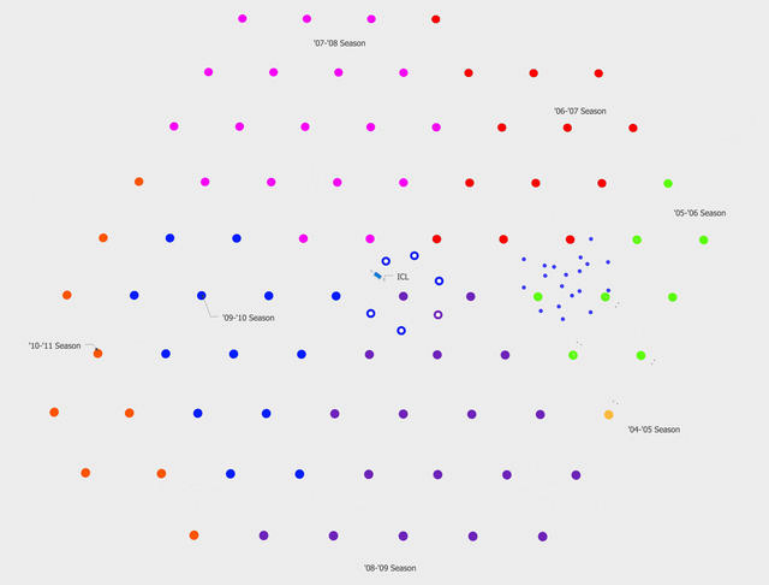

Figure 3.4: The IceCube InIce array. As seen from the top

position of the Sun when we take data. This is useful for the WIMP analysis in distinguishing the signal from the background.

3.2.3 Digital Optical Modules and data acquisition system

The Digital Optical Module is the fundamental building block of the IceCube detector. The DOMs collect light, convert the signal to waveform data, digitise the signal and transfer it to the surface. [33]

The main elements of a DOM are a 25 cm photomultiplier tube (PMT) (Hamamatsu R7081-02) with 20% quantum efficiency, a 2 kV high voltage power supply for the PMT, the DOM Main Board, a stripline signal delay board, a 13 mm thick glass sphere to withstand the pressure of its deep deployment, an RTV gel to provide support and optical coupling from the glass sphere to the PMT, a LED flasher board and a mu metal grid to protect the PMT from the Earth's magnetic field.(See fig. 3.5)

The PMTs efficiency depends on the wavelength of the light. They are most efficient in the blue light where most of the Cherenkov photons are emitted.

The DOMs flasher board hosts 12 LEDs which can be used to send signals to other DOMs. This is done to calibrate distant DOMs, simulate physical events and to investigate optical properties of the ice. In addition the DOM

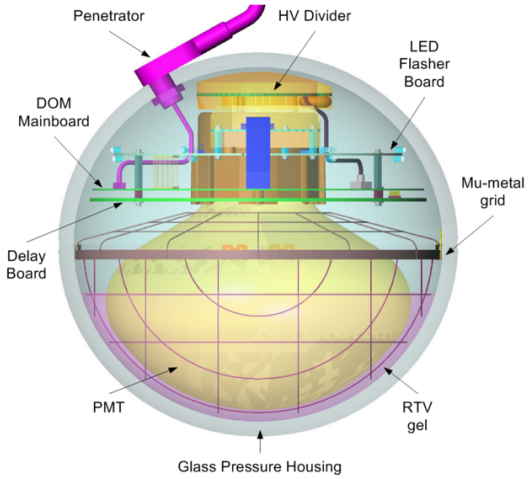

Figure 3.5: The Digital Optical Module

is equipped with an onboard LED which delivers precisely timed, but weak signals for calibration of single photo-electron pulses and PMT transit times.

The DOMs work in the following way. When light hits the photocathode of the DOM the PMT will turn the light signal into an electronic signal. This analog electronic signal will be sent to the main board and divided between the signal delay board and a trigger discriminator. The trigger has a programmable threshold. If the discriminator threshold is surpassed the delayed signal is sent to an Analog Transient Waveform Digitizer (ATWD) and a Fast Analog to Digital Converter (FADC). These digitize the signal into a waveform (See fig. 3.6). The ATWD has four channels. Three channels capture the analog signal with different gains (x16, x2 and x0,25) . The fourth channel can be fed with 8 different signals through external multiplexers. This channel is mostly used for calibration (Clocks, internal LED Pulses, timestamps). To reduce deadtime the DOM's mainboard contains 2 ATWDs which are used in a ping-pong mode. This means after a waveform capture is started on one chip, the next waveform will be captured by the other ATWD. This setup virtually reduces the deadtime of IceCube to 0.

The FADC has only one channel and captures waveforms over a longer time scale of 6400 ns.

There is an additional trigger for the digitization of the signal. DOMs are in contact with their neighbouring DOM. When a DOM gets hit, it sends a Local Coincidence (LC) signal to a neighbouring DOM and opens up a time window of 1μs. If it receives an LC signal of a neighbouring DOM in that time window the local coincidence condition is met. In this way isolated hits,

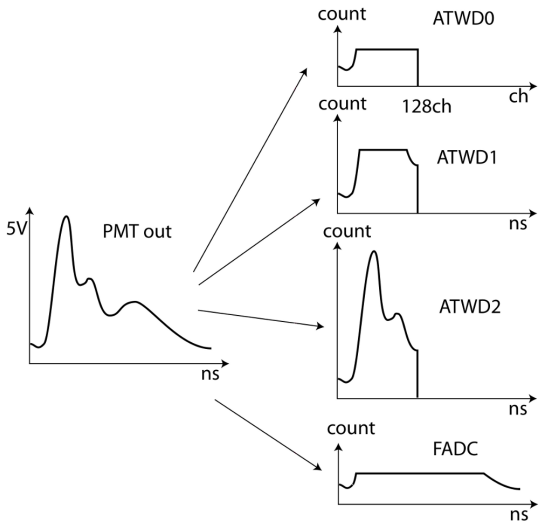

Figure 3.6: The PMT output signal fed to the ATWDs and FADC. Each channel has a different gain and a different saturation level.

which are due to background most of the time aren't digitized and don't take up digitization time. After digitization the signal is sent up to the surface.

Timestamping in the DOMs is done with a free-running high-stability crystal oscillator. This permits the precise time calibration of data without actual synchronization. With this, a time resolution of 2 ns and a low impact on network bandwidth is achieved.

The data acquisition system (DAQ) operates in the following way. The 60 DOMs on a string are connected to the surface through a single cable. The digital information is sent to a Surface Junction Box (SJB) which also gathers information on the 4 DOMs in IceTop above the string. The signal is then sent to the IceCube Laboratory (ICL)(Seen on fig 3.4) through a surface cable. Each string is controlled by a computer called a DOMHub. There is a master clock providing each DOMHub with a high precision internal clock. This masterclock makes use of the GPS system.

3.3 Experimental goals

The IceCube detector will be used for several different purposes related to the fields of astrophysics and/or particle physics. Here we give a list and a brief description.

- Cosmic rays: For most of the studies done with IceCube, cosmic rays

are responsible for the majority of the background. Not everything is known about cosmic rays so they are still interesting for study. The energy spectrum and chemical composition of high energy cosmic rays will be studied with IceTop, a part of the IceCube detector we will describe later on.

- Point sources of high energy neutrinos: These sources could help in the explanation of the highest energy cosmic rays. These cosmic rays have energies high enough that they can not be contained by the galactic magnetic field, so they are believed to have extragalactic origin. Because they do not interact electromagnetically, neutrinos won't be deflected by magnetic fields and would therefore point back towards their source. IceCube is more sensitive to point sources in the Northern hemisphere than in the southern hemisphere, due to the cosmic ray background, using deepcore.

- Gamma ray bursts: When a gamma ray burst occurs (a flashes of gamma rays probably caused by the collapse of a star to a black hole) it should also send out highly energetic neutrinos. Potentially the neutrino flux and the gamma ray flux can coincide in certain sources and these neutrinos may be observed in IceCube.

- Neutrino oscillations: IceCube can observe neutrino oscillations from atmospheric cosmic ray showers. IceCube will be able to put constraints on θ^{23} and if θ^{13} is sufficiently large IceCube would be able to determine the mass hierarchy of the neutrinos, with the deepcore extension.

- Galactic supernovae: Neutrinos from extragalactic supernovaer have energies below the detector energy treshold. But local supernova could be observed as a detector-wide, brief, correlated rise in noise rates.

- Indirect dark matter search: The search for WIMP dark matter, which is explained in this thesis.

Chapter 4

Simulated and experimental data.

4.1 Simulation of data.

In order to analyse the detector data Monte Carlo simulations of the WIMP signal and the background are made. These simulations are used to find a way to distinguish the signal from the background and to determine the sensitivity of the detector. The simulations are made with a Monte Carlo method, which is a collection name for methods using random sampling in a defined domain to compute results. All simulated data used in this thesis was produced with a Monte Carlo method. Simulated data were produced for atmospheric muons, atmospheric neutrinos and neutrinos from the Sun created in the annihilation of neutralinos. There are two simulations made for the atmospheric muons, one for muons from single cosmic ray showers and one for muons from two coïncident showers that look like a single track.

The simultion is done in different steps. The first step is the generation of the events for each type of simulation. The neutrinos and muons are simulated with a given energy and a dirrection. The next step is to simulate the propagation of the muons through the Earth. The last step is the simulation of the detector response.

4.1.1 Generation of events.

Atmospheric Muon events: The simulation of the atmospheric muons is done with the program COsmic Ray SImulations for KAscade (CORSIKA) [34]. This program simulates extensive air showers initiated by high energy cosmic ray particles, protons, light nuclei up to iron, photons, and many other particles. The spectrum of the primary cosmic rays responsible for

the atmospheric muons is derived from other experiments. The higher the energy of the primary particles the more uncertain we are about their spectrum and their interaction in the atmosphere. Because higher energies are harder to produce and study in laboratory experiments. The simulation includes hadronic interactions (using the QGSJET model [35]), decay of unstable particles, ionization and scattering energy losses in the atmosphere, and deflection of charged particles by the Earths magnetic field. CORSIKA was developed by the Forschungszentrum Karlsruhe. The version used in IceCube is called (Dimitry Chirlein's) dCORSIKA [36], which takes into account the curvature of the atmosphere at the South Pole.

The simulation of two muon events forming one track is also made with this program, by generating two airshowers and forcing the resulting muons to both interact in the detector within a time window of a few μs.

The simulated muons have an energy range between 600 GeV and 10^{11} GeV. The simulated sample used in this thesis contains single atmospheric muon envents and coincident atmospheric muon events.The number of simulated single muon events in the analysis is 3263390 event and two muon events is 775076 event.

Atmospheric neutrinos: The program used for the simulation of atmospheric neutrinos is NuGen. This program is used to simulate upgoing and downgoing neutrino events. Since only neutrinos are able to pass through the Earth, only neutrinos have to be considered as primaries for up-going events in IceCube. The NuGen code is based on ANIS, the program used for atmospheric neutrino generation in AMANDA[37]. Neutrino Charged Current interactions were simulated using the CTEQ5 model cross-sections and parton distributions[38].

The number of simulated neutrino events in the analysis is 642446 events.

WIMP neutrinos: The solar WIMPs are simulated with WimpSim[39] a program written by J. Edsjö. This program takes into account all sorts of WIMP annihilation channels through DarkSUSY[40] and PYTHIA[41] calculations. This code calculates the annihilation of WIMPs inside the Sun, collects all the neutrinos that emerge and lets these propagate out of the Sun to the Earth and in the Earth to the detector including neutrino interactions and neutrino oscillations. The oscillation of the neutrinos is calculated in a different way whether they are propagating through the Sun, vacuum or the Earth. The oscillation parameters used were $\theta_{12} = 33.2°$, $\theta_{13} \leq 12.5°$, $\theta_{23} = 45.0°$, $\Delta m^2_{21} = 8.1 \times 10^{-5} eV^2$, $\delta = 0$ and $\Delta m^2_{31} = 2.2 \times 10^{-3} eV^2$. For the muon neutrino charged current cross-section WimpSim uses the program NUSIGMA. Neutrino regeneration from the creation and annihilation of τ

particles is also included. The number of simulated WIMP events is 83212.

In this thesis we only look at neutrinos originating from 1 TeV neutralinos with a hard deacay spectrum (W^+W^-) and 3 TeV neutralinos with a soft decay spectrum ($b\bar{b}$).

4.1.2 Propagation of muons and photons.

After the events are generated, the muons and taus from the atmosphere and those created in neutrino interactions are passed to the Muon Monte Carlo (MMC)[41] program, which calculates the muon propagation and energy losses in the detector and its vicinity. An accurate simulation of the propagation of muons is necesary because a muon can interact hundreds of times before it is detected by the experiment. A small systematic uncertainty repeated hundreds of times can lead to sizable errors. The simulation includes muon decay, bremsstrahlung, photo-nuclear interaction, ionization and scattering. All of the energy losses have continuous and stochastic components. The energy loss due to the emission of Cherenkov light is neglegible. To limit the computation time the the level of detail in the simulation depends on the location of the particle. Outside the sensitive volume of the detector the energy loss is averaged out and approximated as continuous if the energy loss is less than 5%. In the sensitive volume where the light from energy losing processes can reach the detector the simulation is more detailed. For the IC40 detector the sensitive volume is a cylinder around the detector with a heigth of 1600 m and a radius of 800 m.

The simulation of Cherenkov light emission and propagation in the ice is handled by Photonics[43]. This software is used to calculate the photon flux and time distribution in the ice. As mentioned before the ice varies in clarity. Because of this the scattering and absorption depend on the depth of the ice and the wavelength of the photons. In order to mimimise computation time the simulation is done in two stages. Detailed simulations are made of many different particle tracks. The photon intensity and time delay due to scattering for each DOM is stored in tables cooresponding to diffrent directions of the muon particle. A second simulation then randomizes the diffrent particle tracks from the table values.

4.1.3 Detector response.

The response of the detector to the muons is simulated, the programs used calculate in which DOMs the emitted Cherenkov photons would produce a hit. Then the detector response is simulated. Background is added randomly

like dark noise(thermal electrons). The PMT response is simulated using the same algorithms as in the real DOMs the waveform is sampled by the ATWDs and fADCs.

4.2 Experimental data.

Because of the atmospheric muon background we focus the analysis on periods when the Sun is below the horizon. The experimental dataset used in this analysis consists of 17 days of data taken in the year 2008 with an IceCube detector consisting of 40 strings. Starting from the 17th of April until 23th of September. This corresponds to a livetime of 1 372 716 seconds. This is later in the year than usual because the detector wasn't ready until the end of April. The 17 days of data are spread out over the year in angles to account for the different positions of the Sun, or more precisely the diffrence in zenith angle. There are two reasons why this is done. With different Sun positions the WIMPs need to travel more of the Earth. A second reason is that for different Sun positions the WIMPs enter the detector from a different angle. This will change the observables we measure in an event figure 4.1 shows the different Sun positions of the dataset used as function of the detector lifetime. The experimantal data consists out of 29929061 event.

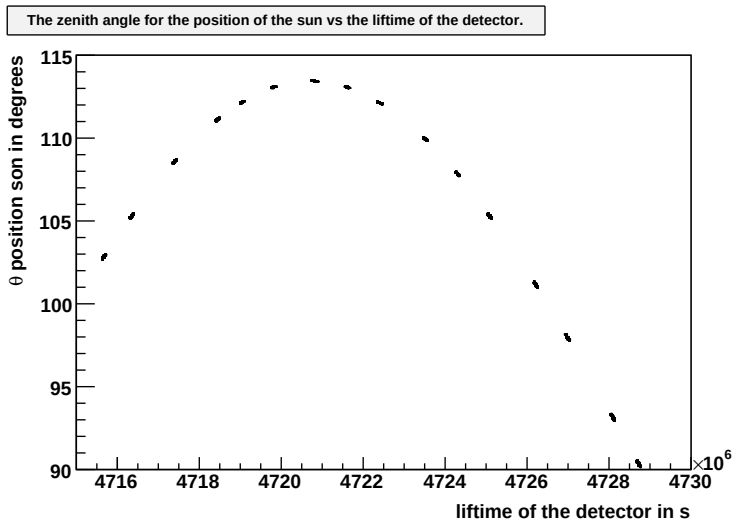

Figure 4.1: The zenith angle of the position of the Sun vs the time of data taking.

A problem with the reconstruction of muon tracks is that downgoing tracks can be reconstructed as upgoing tracks. This happens more for low

energy events because less DOMs are hit in these events. This is also simulated.

Chapter 5

Analysis

In this chapter all the steps needed to filter out the background while retaining neutralino WIMP signal will be described. In this thesis we look for neutralinos with a 1TeV mass which decay through a hard channel(W^+W^-) and neutralinos with a 3 TeV mass which decay through a soft channel($b\bar{b}$). The muon energy spectrum of both are shown in figure 5.1 For the optimiza-

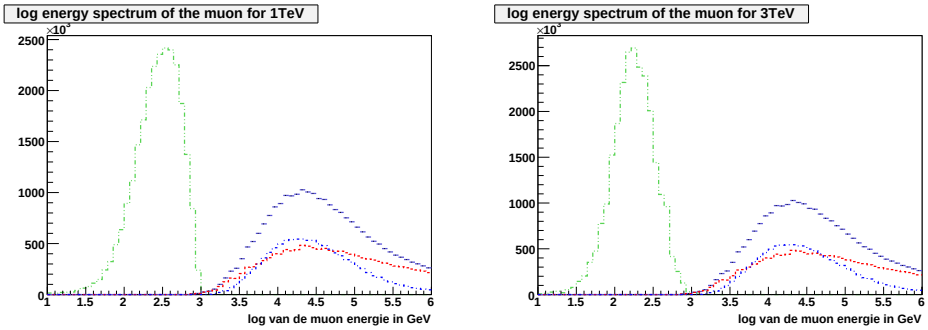

Figure 5.1: The muon energy spectrum at filter level 2 for the 1TeV hard decaying channel and the 3 TeV soft decaying channel. The figures show the WIMP signal (green, dash-dotted), the total simulated background (dark blue, dashed), the single muon background (light blue, dotted) and the coincident muon background(red, dotted).

tions of the filter we used simulated neutrinos, simulated atmospheric muons and simulated atmospheric coincident muons, the simulation is described in chapter 4.

5.1 Reconstruction

5.1.1 Feature extraction

From the waveform in the ATWDs and the fADC, information is extracted in order to reconstruct the tracks.[44] The reconstruction is the basis of all analysis of IceCube data. The process of extracting pulses out of the waveform and the information they provide is called feature extraction. Before the feature extraction can be done the output of the three channels of the ATWD have to be merged and calibrated. This is done by taking the waveform bins of the lowest unsaturated channel and combining them. The feature extraction is done differently for IceTop DOMs and InIce DOMs. IceTop data isn't used in this thesis so will only discuss InIce. In InIce a fast iterative Bayesian unfolding method is used, because it is both fast in execution and precise. The technique assumes that we know the shape for a single photon (SPE, or single photo-electron pulse), extracts information from the largest peak and then iteratively creates a function to approximate the waveform. When the waveform has been fitted, the leading edge of the pulse is followed down to the baseline value of the DOM. The crossing point or the leading edge time is used as an estimate of the photon arrival time. The area below the fitted function gives an estimate of the integrated charge response.

5.1.2 Track reconstruction

Using the hit pattern of an event an estimation of the track can be made. Tracks are defined as a line with coordinates zenith θ and azimuth ϕ passing through a point r_0 at time t_0. Initially, simple algorithms are used Although they are not very precise, they can be used as seeds for more advanced algorithms. In the analysis of this thesis the linefit is used as a first guess algorithm[45]. The linefit ignores the geometry of the Cherenkov cone and the optical properties of the medium and assumes light traveling with a velocity $\mathbf{v}$ along a one-dimensional path through the detector. The locations of each DOM, $\mathbf{r}_i$, which is hit at a time $\mathbf{t}_i$ can be approximated by a line $\mathbf{r}_i \approx \mathbf{r} + \mathbf{v} \cdot t_i$. Minimizing

$$\chi^2 = \sum_{i=1}^{N_{hit}} (\mathbf{r}_i - \mathbf{r} - \mathbf{v}t_i)^2 \tag{5.1}$$

where N_{hit} is the number of hits in an event, gives the solution.

$$\mathbf{v} = \frac{\langle \mathbf{r}_i t_i \rangle - \langle \mathbf{r}_i \rangle \langle t_i \rangle}{\langle t_i^2 \rangle - \langle t_i \rangle^2} \tag{5.2}$$

and

$$\mathbf{r} = \langle \mathbf{r}_i \rangle - \mathbf{v} \langle t_i \rangle \tag{5.3}$$

So the linefit gives us a vertex point $\mathbf{r}$ and a direction $e = \frac{\mathbf{v}}{|\mathbf{v}|}$. The absolute velocity $|\mathbf{v}|$ of the line-fit is the mean velocity of the light propagating through the one-dimensional detector projection. Usually this is different from the lightspeed in vacuum.

A more precise track reconstruction is obtained with the maximum log likelihood method. The implementation of the likelihood method requires detailed knowledge of the photon propagation in the ice. The photon hit probabilities and arrival time distributions can be simulated as functions of all relevant parameters with a dedicated Monte Carlo simulation and archived in large look-up tables. Using these tables however isn't very efficient for computing. Therefore the distributions in the look up tables are parameterized with analytical functions using only a subset of parameters. This is done with the Pandel function

$$p(t_{res}) \equiv \frac{1}{N(d)} \frac{\tau^{-(d/\lambda)} \cdot t_{res}^{d/\lambda - 1}}{\Gamma(d/\lambda)} \cdot e^{-\left(t_{res}\left(\frac{1}{\tau} + \frac{c_{medium}}{\lambda_a}\right) + \frac{d}{\lambda_a}\right)} \tag{5.4}$$

$$N(d) = e^{-d/\lambda_a} \left(1 + \frac{\tau c_{medium}}{\lambda_a}\right)^{-d/\lambda} \tag{5.5}$$

which gives a distribution of the residual time[45], where λ_a is the absorption length, c_{medium} is the speed of light in the medium, d is the perpendicular distance from the DOM to the track and λ and τ are free parameters. The residual time is the difference between measured time and geometric time, the straight path arrival time of Cherenkov photons. The λ and τ parameters are fit from the photon propagation simulation, for a wide range of distances. A comparison for two distances between the Pandel function and the Monte Carlo simulation is shown in fig. 5.2. The Pandel function is also convoluted with a Gaussian function to take into account random detector noise and PMT jitter. The likelihood is then given by

$$L = \prod_{i=0}^{N} p(t_{res}) \tag{5.6}$$

where N is the number of hits in an event and the negative logarithm of the likelihood *llh* is $llh \equiv -log(L)$. The negative logarithm is taken because a minimum is easier to compute than a maximum. The log likelihood (LLH) track fit is then found by varying the track hypothesis and minimizing *llh*.

Because several minima can occur in the available phase space, the first guess track is used to find the correct minimum. [45]

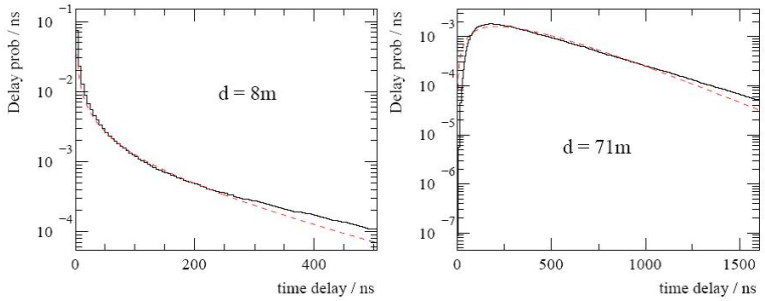

Figure 5.2: Comparison of the parametrized Pandel function (dashed curves) with the detailed simulation (black histograms) at two distances d from the muon track.[45]

When a minimum is found in the likelihood function a parabola is fit around it. The width of the parabola gives an estimation of the reconstruction error of the track. Doing this in two dimensions gives us two error estimations σ_θ and σ_ϕ for each of the axes from which a single parameter is derived. $\sigma_{llh} = \sqrt{\frac{\sigma_\theta^2+\sigma_\phi^2}{2}}$. In general the smaller σ_{llh}, the better the track fit.

Direct hits of class C (dir c hits) are hits with t_{res} falling in a time window between -15 ns and 75 ns.

The track information and the collected hit information are used to calculate observable quantities which are used in the analysis. Here we give a list and a brief description of each variable.

- n_{ch}: The number of channels or DOMs with a hit in an event.
- z_{trav}: The mean z displacement from the z average calculated from all channels and the z average calculated from the first quartile of channels.
- θ: Zenith angle of the linefit reconstruction track.
- θ_{llh}: Zenith angle of the LLH reconstruction track.
- t_{ext}: The duration of an event the time between the first hit in an event and the last hit.

- ψ_{diff}: The opening angle between the linefit and the LLH track reconstruction.
- σ_{llh}: The width of the log likelihood optimum found from a parabola fit.
- s_c: The number of strings with direct hits of class c.
- ρ_{avr}: The mean perpendicular distance from the LLH track to the hit DOMs.
- $COGz$: The mean z coordinates of channels weighted with the charge in each hit DOM.
- l_c: The maximum length between two direct hits of class c.

5.2 The effective volume and generation volume.

Here we describe two quantities: the effective volume and the generation volume.

During simulation of WIMP events, the interaction vertices are spread in a volume around the detector array, which is known as the generation volume. It is defined as a box around the detector with a length L along the neutrino track and the projected area of the sensitive volume as cross section. The generation volume is different for each event and depends on that event's energy. When we look at the ecolution of the average generation volume with cuts at level three we 'll see that it increases because the low energy events are cut away more.

The effective volume V_{eff} is a measurement of the efficiency of the detector in detecting a neutralino WIMP signal. It is derived from WIMP simulations. Consider an ideal experiment that monitors a volume V during a time t. With ideal we mean that every WIMP neutrino with a muon flavor interacts and produces a muon in the volume V and that muon is triggered in the detector, reconstructed, and selected at the final cut. Unfortunately we don't have an ideal detector. Each of the components in the detector has a non perfect efficiency, which degrades the sensitivity to the neutralino induced neutrino flux.

In our calculation of the effective volume we take into account that the generation volume for each simulated event differs. This is important because

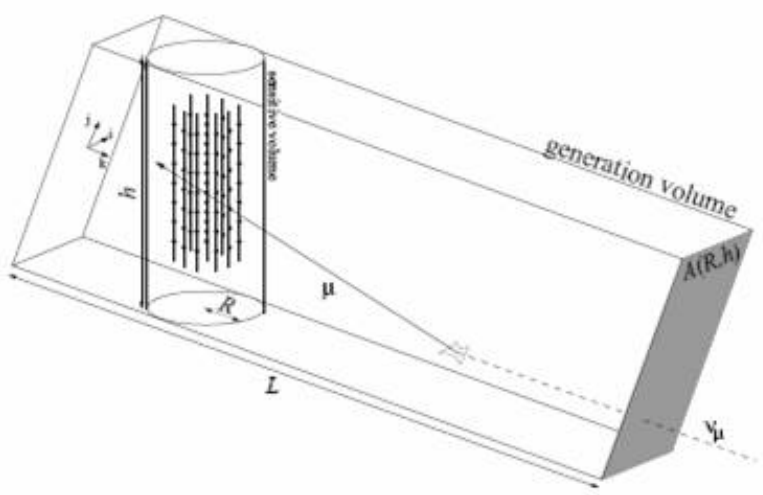

Figure 5.3: The generation volume, determined by its length L and the sensitive cylinder around the detector array. Adapted from[46]

high energy events have a higher chance of being detected and so have a higher efficency. The high energy events dominate the detector efficiency. So the formula used to calculate the effective volume is

$$V_{eff} = \left\langle \frac{N_{sel}}{N_{gen}} \times V_{gen} \right\rangle = \frac{\sum_{i=1}^{N} w_i \delta_i V_{gen,i}}{\sum_{i=1}^{N} w_i} \tag{5.7}$$

where w_i is the weight of an event, δ_i is either 1 or 0 if the event is selected or not and $V_{gen,i}$ is the size of its generation volume. The weight stored for an event consists out of different pieces of information for the different processes in the generation: the propagation through the earth and the absorption of the neutrino and the energy dependence of the cross section.[47]

5.3 Filter levels one and two

The analysis can be divided into different consecutive levels. The first level of the analysis is performed at the filtering farm at the South Pole. All recorded events were cleaned of bad DOMs, feature extracted, and fitted. Cuts are then placed on the data to reduce the amount that needs to be sent over by satellite, which is limited in bandwidth. A good filter is therefore necessary considering than the detector is still growing which results in a higher trigger rate. For this analysis the ICMuonfilter of 2008 was used. The purpose of this filter is to efficiently remove down going muon background while retaining as many useful signal events as possible. It is useful in many

analyses. The basic filter consists of two branches of cuts and a minimum n_{ch} threshold of 10. Both branches are necessary and complement each other. The first branch has the following cuts

$$\theta_{llh} \geq 70^{\circ}$$
$$n_{ch} \geq 10$$

and the second branch has

$$\frac{n_{hits}}{n_{ch}} \geq 5$$
$$\theta_{llh} \geq 50^{\circ}\ with\ n_{ch} \geq 20$$
$$or$$
$$\theta_{llh} \geq 70^{\circ}\ with\ n_{ch} \geq 10$$

the θ_{llh} observable used by this filter is different from the one used later in the analysis, because at this level another LLH fit is used. The LLH fit used here uses a SPE Pandel function, with one iteration seeded by the linefit.

After these cuts are made the data is sent over with the satellite. At level 2 the waveforms are again feature extracted, cleaned for bad DOMs and hits outside a time window of 6 μs are removed. The tracks are fitted with a linefit track and subsequently fitted with a LLH fit, this time a MPE Pandel function with an 8-iteration SPE fit as seed. The LLH minimum is fitted with a parabola. No cuts are made at this level.

The simulated and the experimental data were compared. At this level of filtering we expect that the data are dominated by atmospheric muon background. Three parameters did not match the simulation completely. The first two parameters are the zenith angle of the linefit and the LLH fit.

In figure 5.4 it can be seen that the simulated background data and the experimental data don't match between 50 and 70 degrees; this is the same for the linefit and the LLH fit. The second branch in the muonfilter makes different cuts in that region. It is possible that one of the underlying parameters differs here. This region is cut away at level three so it should not give any problems in the analysis.

The third parameter where the simulated data and the experimental data don't match very well is the center of gravity of the z coordinate(COG z). In figure 5.5 it can be seen that in the deeper parts of the ice the simulated data underestimates the amount of events and in the top layers of the IceCube detector the amount of events are overestimated. There is a dip in the middle part of the detector due to the dustlayer. The underestimation in the bottom layers can be due to a poor modelling of the ice in those layers which is clearer than the upper layers. The overestimation in the top layers could be due to

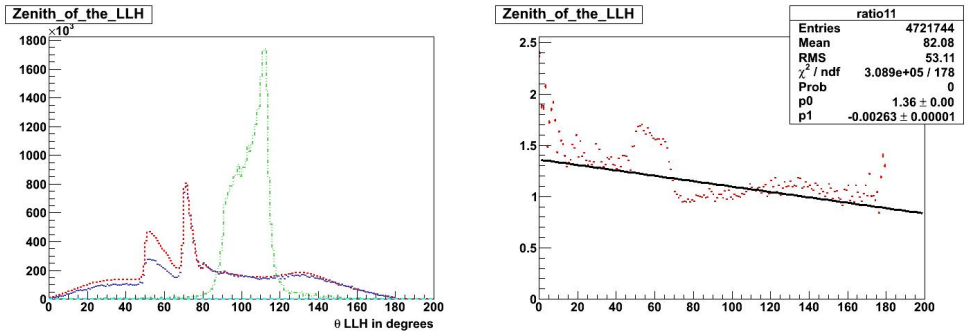

Figure 5.4: The figure on the left is the distribution of θ_{llh} for the experimental data (red dotted) the simulated data (blue, dashed) and the WIMP signal from the Sun (green, dash-dotted). The figure on the right shows the ratio of the experimental data and the simulated data with a line fitted through them. The experimental data is divided by the simulated data.

an overestimation of the coincident muon background events in the top layers. This is a known effect in IceCube simulation and much collaboration effort is being spent to reduce the differences for future analyses.

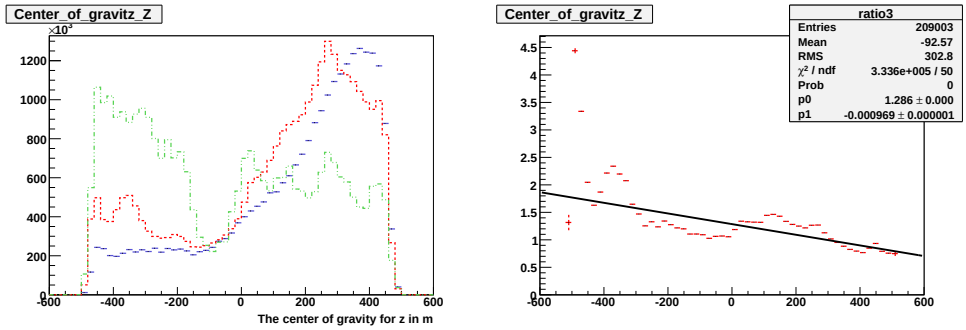

Figure 5.5: The figure on the left is the distribution for COGz with the experimental data (red, dotted) the simulated muon data (blue , dashed) and the WIMP signal from the Sun (green, dash-dotted). The figure on the right shows the ratio of the experimental data and the simulated background data with a line fitted through them, the experimental data is divide by the simulated data.

The values for the average generation volume, the effective volume and the average muon energy for the WIMP signal are given in Table 5.1. The rates for the diffrent kinds of data at level 2 are given in table 5.2. The diffrent observables at level 2 are shown in figure 5.6.

5.4 Analysis level three.

At the third analysis level cuts are made specifically to optimise the efficiency to find solar WIMPs. This analysis is the contribution of this thesis. Its purpose is to separate the WIMP signal from the background and estimate the sensitivity of the detector. Ten observables were used to cut on. These observables were selected for their separation power from a list of observables. Some of the observables were used in a previous IceCube dark matter study with the 2007 (IC22) data (Gustav Wikström[48]). There are two kind of cuts made; those made on one-dimensional histograms and those made on two dimensional ones to benefit from the correlation between parameters.

A selection criterium was investigated for aplication to the one dimensional in order to estimate the best cut. This criterium uses the following function to estimate the efficency of a cut

$$\chi = \frac{N_{sigcut}}{N_{sig}}(1 - \frac{N_{backcut}}{N_{back}}) \tag{5.8}$$

where N_{sigcut} is the amount of signal events after the cut, N_{sig} is the amount of signal events before the cut, $N_{backcut}$ is the amount of simulated background events after the cut and N_{back} is the amount of simulated background events before the cut. The ideal cut according to the criterium is then made where χ reaches an absolute maximum. This criterium was almost never followed. We thought that the criterium proposes a cut that is too hard when there is a steep rise in the histogram and a cut that is too conservative when there is a long tail in the histogram.

The cuts made in this analysis are the same for the 1 TeV hard signal and the 3 TeV soft signal until the final angular resolution cut. After level two, 59.1% of the 1TeV and 46.3% of the 3TeV simulated WIMP signal was kept.

In the following a detailed description is given of the filter for the 1 TeV hard signal. From this point on all ratios will be quoted with respect to level two to be in agreement with the experimental data we are using in this analysis. An overview of the efficiency at each cut level is given in table 5.6.

The first step consisted of the removal of all the events where their was a computer error in the mathematical computation of the track or the parabola fit.

Table 5.1: The average generation volume, the effective volume and the average muon energy for WIMPs at level 2 with failed reconstructions removed.

m_{chi} (TeV)	Channel	$\langle V_{gen} \rangle$ (km^3)	V_{eff} (km^3)	$\langle E_\mu \rangle$ (GeV)
1	hard	7.43	0.118	229.7
3	soft	6.31	0.025	209.6

Table 5.2: The rates of the simulated and the experimental data at level 2 with bad reconstructions removed.

rate Atm ν_μ Hz	rate Single atm μ Hz	rate Coinc atm μ Hz	Sum of atm backg. Hz	rate Exp Hz
0.0035	10.50	8.07	18.57	18.73

The plots of all the variables used in the filter are shown in figure 5.6 before cuts and in figure 5.15 after all cuts for 1 TeV hard. The first cuts (cut1) that are made are on the 2 dimensional zenith histogram (see fig 5.7). A cut on the zenith of the muon tracks is the first cut made because it has a clear physical basis. One of the clearer ways in which the WIMPs distinguish themselves from the background is the direction from which they enter the detector, namely from the position of the Sun. As can be seen on the 2 dimensional zenith angle distribution in fig 5.7 , the WIMP signal can be selected more accurately by making four diagonal cuts. The zenith angular cuts are made at

$$\begin{aligned} 85^\circ < \theta_{llh} < 130^\circ \\ \theta \leq (-19/8)\theta_{llh} + 440^\circ \\ \theta \leq (78/29)\theta_{llh} - 99^\circ \\ \theta \geq (62/55)\theta_{llh} - 61^\circ \\ \theta \geq (-21/16)\theta_{llh} + 175^\circ \end{aligned}$$

Afther these cuts 94.8% of the WIMP signal, 23.2% of the simulated background and 19.6% of the experimental data was retained. The θ_{llh} cut was set at 85° to cut away a high peak of background as seen on fig 5.6. This cut gets rid of obvious background which gives us a better view of the other observables in the analysis.

The second cut (cut2) is made on z_{trav} (see fig 5.9). Of all the observables this one had the best separation power. Its therefore used as the second cut to get as much of the easily distinguishable background removed. This observable makes a distinction between up going and down going tracks. The

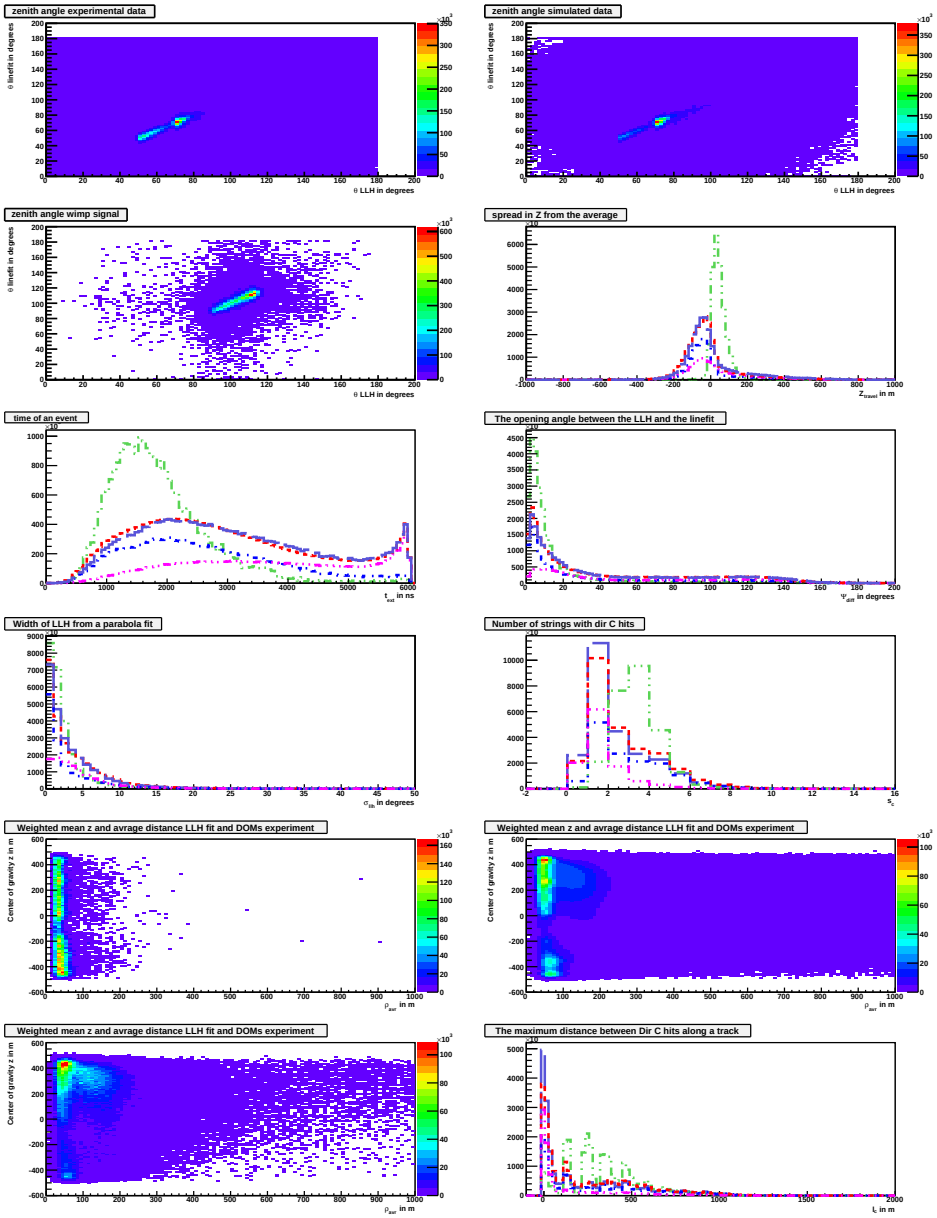

Figure 5.6: Distribution of observables at level 2 for the experimental data (red, dotted), the simulated signal 1TeV hard WIMP (green, dash-dotted) and background. The total background (dark blue, dashed), is the sum of atm single μ (light blue, dotted), atm coincident μ(purple) and atm ν_μ. Left column from the top: θ vs θ_{llh} exp, θ vs θ_{llh} WIMP, t_{ext}, σ_{llh}, COG z vs ρ_{avr} WIMP,COG z vs ρ_{avr} atm background. Right column: θ vs θ_{llh} atm background, z_{trav}, Ψ_{diff}, s_c,COG z vs ρ_{avr} exp, l_c

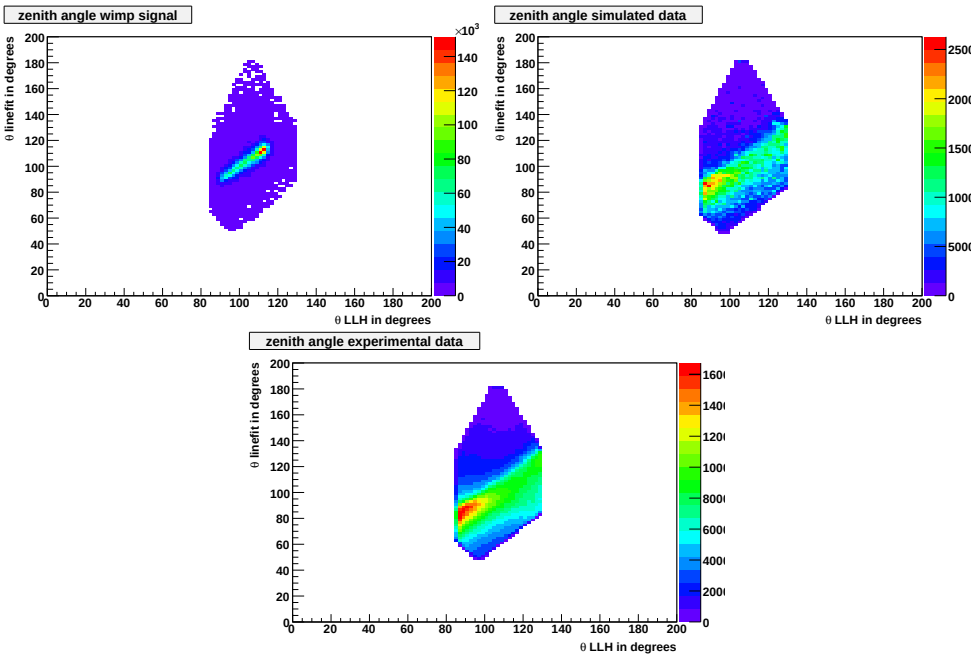

Figure 5.7: Two dimensional histograms of the zenith angle: on the y axis the zenith angle of the linefit and on the x axis the zenith angle of the LLH fit, after cut1. The upper left plot shows the WIMP signal, the upper right plot shows the simulated background and the bottm plot shows the experimental data.

cuts are made at $-5m \leq z_{travel} \leq 160m$. After these cuts 90.3% of the WIMP signal, 9.6% of the simulated background, and 8.7% of the experimental data was kept.

The third cut (cut3) is made on t_{ext} the duration of an event (see fig 5.9). This is the time between the first DOM in the event being hit and the last DOM being hit. This observable is good for removing coincident events when cut on the right, because a single particle needs a shother time (about 3 μs) to travel through the detector than it would take for two intersecting particles to travel both through the detector. The cut is made at $400ns \leq t_{ext} \leq 3200ns$. After this cut 85.3% of the WIMP signal was kept, 5.4% of the simulated background and 5.4% of the experimental data. When this cut is made the coincident background rate goes from 1.04 Hz to 0.48 Hz

The fourth cut (cut4) is made on Ψ_{diff} the opening angle between the direction of the linefit and the LLH fit (see fig 5.10). This is a first track quality cut, the second one being the next cut. For this observable the back-

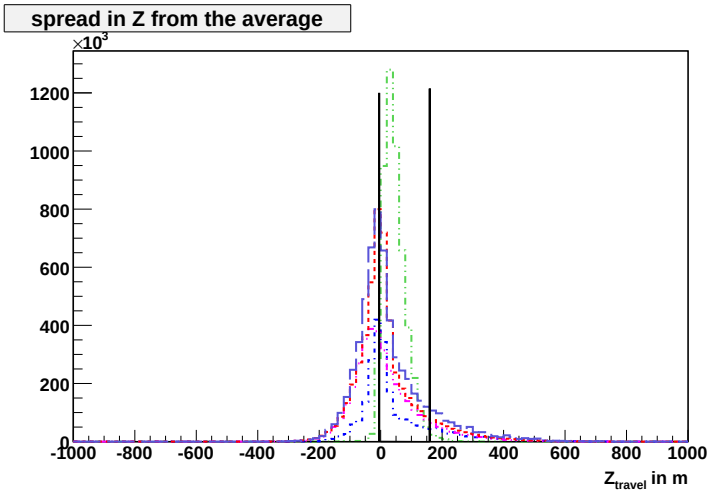

Figure 5.8: Histogram of z_{travel} for WIMP(green, dash-dotted), experimental data (red, dotted) and background. The total background (dark blue, dashed), is the sum of atm single μ (light blue, dotted), atm coincident μ(purple , dotted) and atm ν_μ, after cut1. The verticle lines show the limits of cut2

ground distribution has a longer and thicker tail. This allows us to get rid of background at the cost of loosing low quality WIMP tracks. The cut is made at $\Psi_{diff} \leq 22°$. After this cut 75.3% of the WIMP signal was kept, 2.40% of the simulated background and 1.92% of the experimental data.

The fifth cut (cut5) is made on σ_{llh}, the width of the parabola fit (see fig 5.11). This is the second quality cut. Normally quality cuts would be the first to be made, but keeping them until this point shows that is reasonable to make the cut this hard. The cut is made at $\sigma_{llh} \leq 4.5°$. After this cut 69.8% of the WIMP signal was kept, 1.66% of the simulated background and 1.17% of the experimental data.

The sixth cut (cut6) is made in n_c, the number of direct hits of class c (see fig 5.12). This cut removes a large amount of background but also quite an amount of signal. However this observable still has a lot of separation power after the previous five cuts. The cut is made at $n_c > 2$. After this cut 51.3% of the WIMP signal was kept, 0.044% of the simulated background and 0.045% of the experimental data.

The seventh cut (cut7) is made on a 2-dimensional histogram of the observables ρ_{av} and COGz (see fig 5.13). These two were put together be-

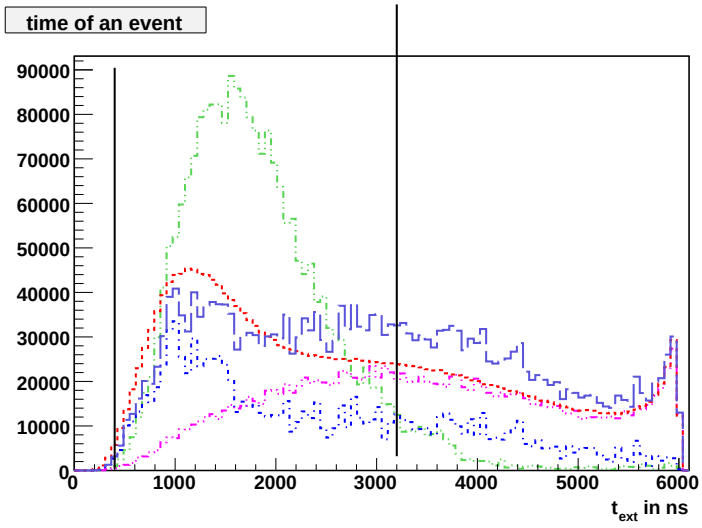

Figure 5.9: Histogram of t_{ext} for WIMP(green, dash-dotted), experimental data (red, dotted) and background. The total background (dark blue, dashed), is the sum of atm single μ (light blue, dotted), atm coincident μ(purple , dotted) and atm ν_μ, after cut2. The verticle lines show the limits of cut3

cause they are highly correlated. The cuts are made at $\rho_{av} \leq 60m$ and COG z $\leq -5.5\rho_{av} + 305.104m$. After these cuts 33.7% of the WIMP signal was kept, 0.0115% of the simulated background and 0.0168% of the experimental data. The $\rho_{av} \leq 60$ cut does very little at this point; the COG z $\leq -5.5\rho_{av} + 305.104m$ selection is made to remove coincident background. Most of the coincident background is in the top layers of IceCube, with this cut the coincident background rate goes from $2.66 \cdot 10^{-3}$ Hz to $1.02 \cdot 10^{-4}$ Hz.

The eighth cut and final cut (cut 8) of level 3 is made on l_c (see fig 5.14). This cut also removes a lot of background. If this cut had been one of the first cuts it would also cut away a lot of signal. The cut is made at $l_c \geq 210m$. After this cut 32.7% of the WIMP signal was kept, 0.0069% of the simulated background and 0.0091% of the experimental data.

If we look at the ratio of the simulated WIMP signal events kept at the end of level 3 in comparison to the signal events at generation level 19.34% is kept for the 1 TeV hard channel and 15.02%for the 3 TeV soft channel. For the experimental data 2339 events out of the 83212 events at level 2 remain.

Table 5.3: The average generation volume, the average effective volume V_{eff} and the average muon energy, after each cut for the 1TeV hard channel.

cut level	$\langle V_{gen} \rangle$ (km^3)	V_{eff} (km^3)	$\langle E_\mu \rangle$ (GeV)
cut1	7.49	0.112	229.7
cut2	7.53	0.106	209.6
cut3	7.47	0.101	229.7
cut4	7.56	0.088	209.6
cut5	7.59	0.082	229.7
cut6	7.70	0.060	209.6
cut7	7.65	0.040	229.7
cut8	7.67	0.039	209.6

Table 5.4: The rates of the simulated and the experimental data at diffrent cut levels.

cut level	rate Atm ν_μ Hz	rate Single atm μ Hz	rate Coinc atm μ Hz	Sum of atm backg. Hz	rate Exp Hz
cut1	0.0022	1.67	2.64	4.31	3.66
cut2	0.0018	0.75	1.04	1.80	1.63
cut3	0.0017	0.53	0.48	1.00	1.02
cut4	0.0014	0.16	0.28	0.44	0.35
cut5	0.0013	0.107	0.20	0.31	0.22
cut6	0.0009	0.0046	0.0027	0.0082	0.0085
cut7	0.0006	0.0015	0.0001	0.0021	0.0031
cut8	0.0005	0.00066	$6.8 \cdot 10^{-5}$	0.0013	0.0017

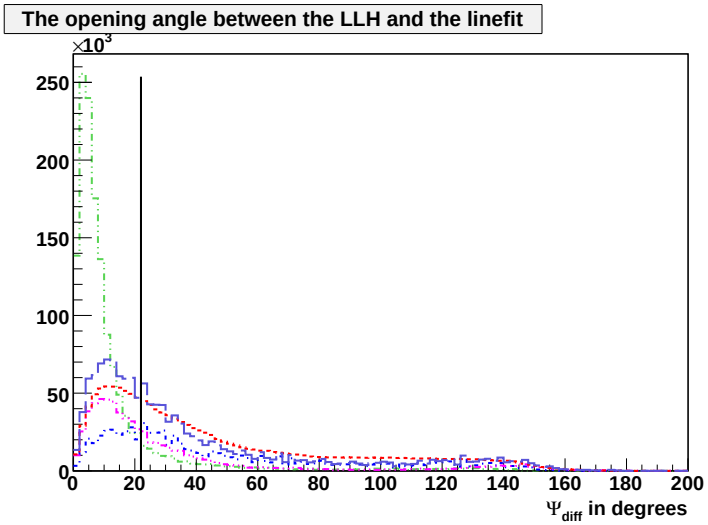

Figure 5.10: Histogram of Ψ_{diff} for WIMP(green, dash-dotted), experimental data (red, dotted) and background. The total background (dark blue, dashed), is the sum of atm single μ (light blue, dotted), atm coincident μ(purple , dotted) and atm ν_μ, after cut3. The verticle lines show the limits of cut4

Table 5.5: The average generation volume, the average effective volume and the average muon energy for WIMPs after all cuts have been made.

m_{chi} (TeV)	Channel	$\langle V_{gen} \rangle$ (km^3)	V_{eff} (km^3)	$\langle E_\mu \rangle$ (GeV)
1	hard	7.67	$39 \cdot 10^{-3}$	344.6
3	soft	6.59	$8.4 \cdot 10^{-3}$	231.5

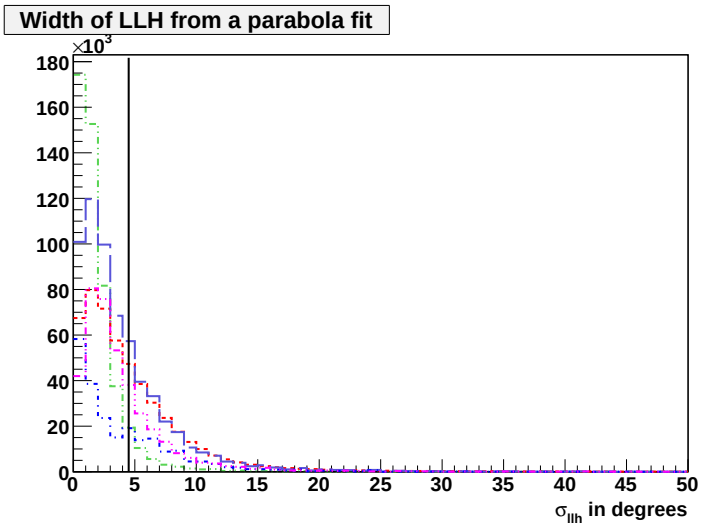

Figure 5.11: Histogram of σ_{llh} for WIMP(green, dash-dotted), experimental data (red, dotted) and background. The total background (dark blue, dashed), is the sum of atm single μ (light blue, dotted), atm coincident μ(purple , dotted) and atm ν_μ, after cut4. The verticle lines show the limits of cut5

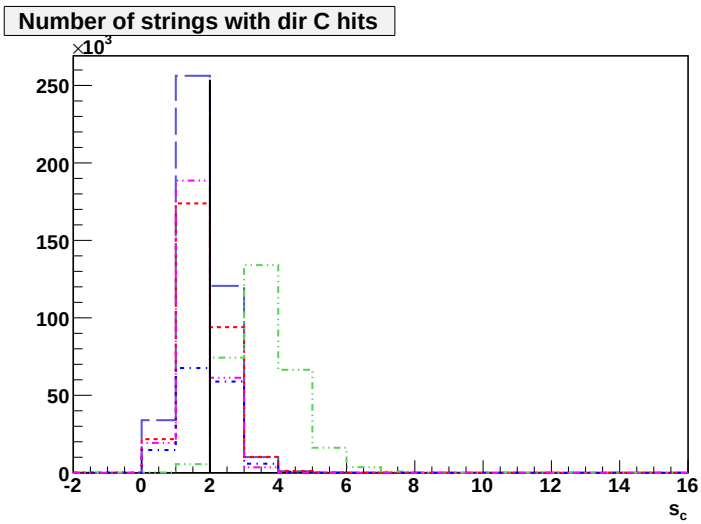

Figure 5.12: Histogram of n_c for WIMP(green, dash-dotted), experimental data (red, dotted) and background. The total background (dark blue, dashed), is the sum of atm single μ (light blue, dotted), atm coincident μ(purple , dotted) and atm ν_μ, after cut5. The verticle lines show the limits of cut6

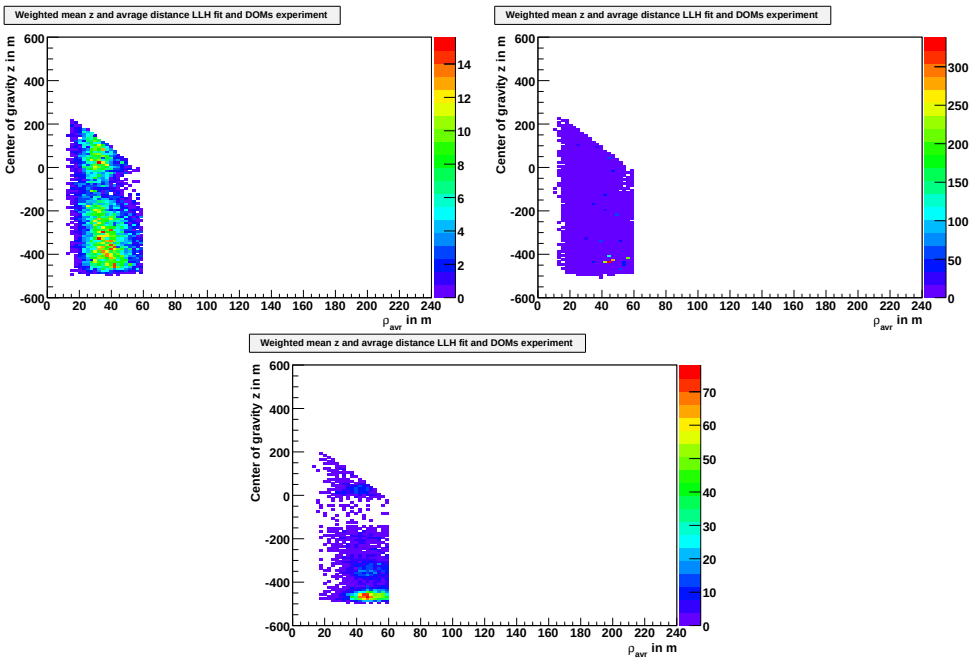

Figure 5.13: Two dimensional histograms on the y axis the COG z and on the x axis ρ_{av}. The left shows the WIMP signal, the right one shows the simulated background and the bottem one shows the experimental data.

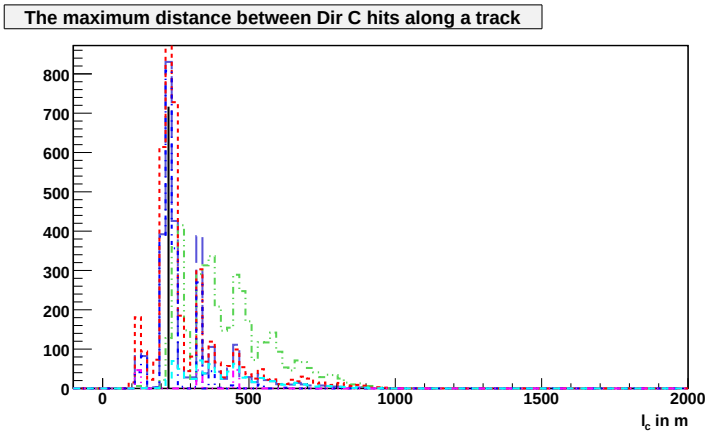

Figure 5.14: Histogram of l_c for WIMP(green, dash-dotted), experimental data (red, dotted) and background. The total background (dark blue, dashed), is the sum of atm single μ (light blue, dotted), atm coincident μ(purple , dotted) and atm ν_μ, after cut7. The verticle lines show the limits of cut8

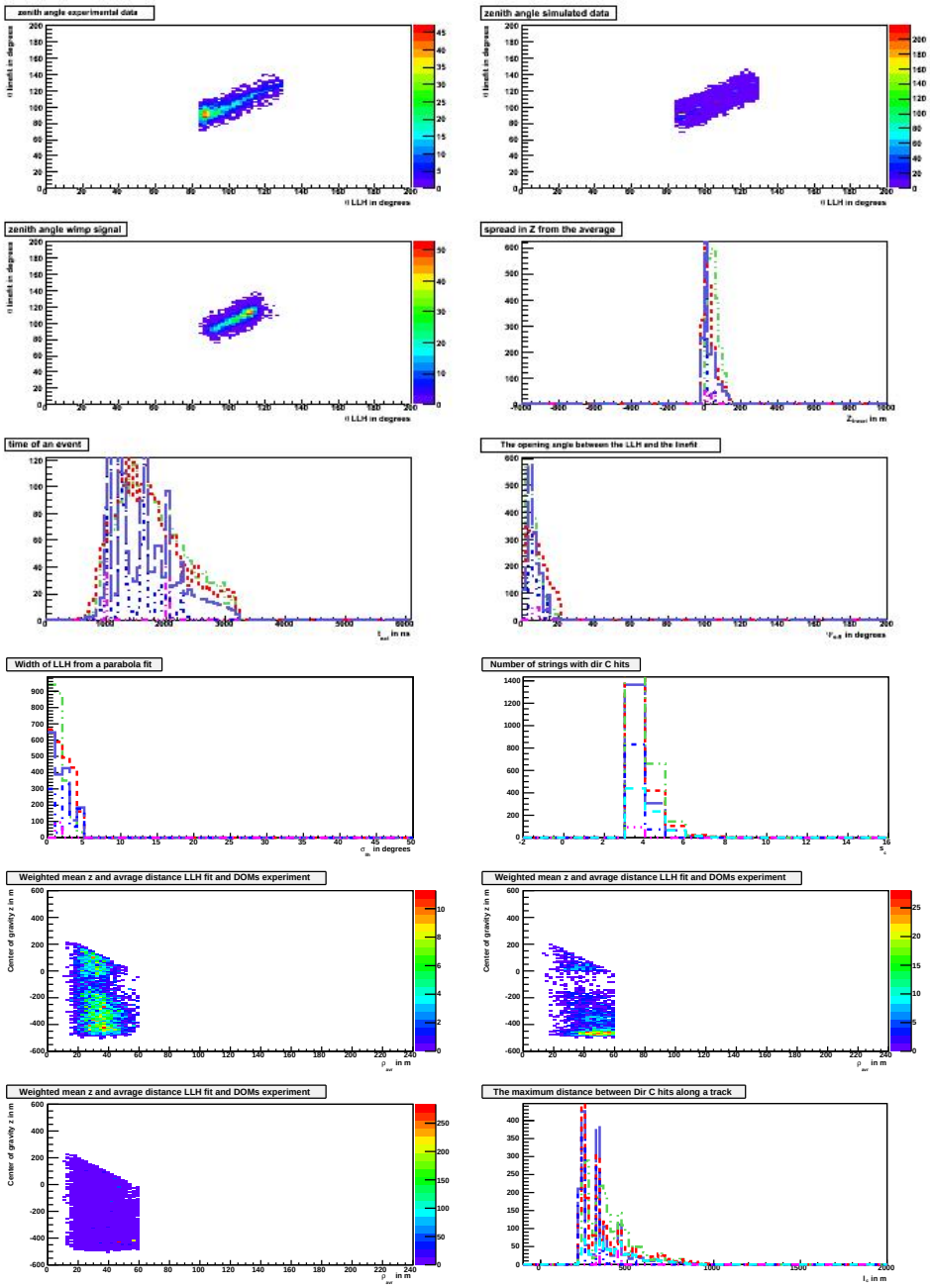

Figure 5.15: Distribution of observables after all the cuts have been made for the 1 TeV WIMP signal for the experimental data (red), the simulated signal (green) and background. The total background (dark blue, dashed), is the sum of atm single μ (light blue, dotted), atm coincident μ(purple) and atm ν_μ. Left column from the top: θ vs θ_{llh} exp, θ vs θ_{llh} WIMP, t_{ext}, σ_{llh}, COG z vs ρ_{avr} WIMP,COG z vs ρ_{avr} sim. Right column: θ vs θ_{llh} sim, z_{trav}, Ψ_{diff}, s_c,COG z vs ρ_{avr} exp, l_c

Table 5.6: The ratio of the retained data with repect to level 2 with the failed reconstruction removed for the 1TeV WIMP signal, simulated background and experimental data.

cut level	ratio WIMP %	ratio sim. background %	experimental data %
cut1	94.8	23.2	19.6
cut2	90.2	9.63	8.69
cut3	85.3	5.41	5.43
cut4	75.3	2.4	1.92
cut5	69.8	1.65	1.17
cut6	51.3	0.044	0.045
cut7	33.7	0.011	0.017
cut8	32.7	0.0069	0.0091

5.5 Angular resolution.

The final cut we make is a cone around the Sun. This cone makes use of our knowledge of the position of the Sun. This cut is made to select WIMP like events from the Sun. This is done last because if it had been done before the level three cuts any signal would have drowned below the background. Due to the requirement of unblinding, the azimuth of the Sun position is unknown during the analysis. This is done to prevent the introduction of a bias by the researcher. During an analysis it's quite possible that small errors are made and certain things are overlooked. If a researcher is allowed to look at the end result of his analysis and has a certain outcome in mind he can go back to the analysis to remove errors and recheck for possible oversights. But if he does this until his results check out with what he expects and stops removing errors then he will have introduced a bias because its very well possible that he did not remove all the errors and oversights in his analysis. Therefore a researcher must check his work thoroughly before he looks at his final result. This analysis has not been unblinded. Instead of the exact position of the Sun the anti azimuth is used to construct a cone, the azimuth position of the Sun + 180°. The angular resolution is the median angular difference between the direction of the reconstructed track and the actual neutrino direction. It can be seen as quality measurement for the track reconstruction. The angular resolution is determined for the WIMP simulated data and an equivalent is calculated for the experimental data. Instead of a true track the position of the Sun is used. In both cases the inner product in spherical coordinates is used

$$\Psi = \arccos(\sin(\theta_1)\sin(\theta_2)\cos(\phi_1 - \phi_2) + \cos(\theta_1)\cos(\theta_2)) \tag{5.9}$$

to determine the space angle between the true track or sun position and the reconstructed one. In the simulated WIMP data the true neutrino direction is used, such that the difference in direction between the neutrino and the muon track is taken into account. The Ψ distributionis shown in fig 5.5. For the experimental data we don't have the true neutrino track, the position of the Sun is used instead. Both the angular cut for 1 TeV and 3 TeV are made so that 90% of the final WIMP signal is kept. For 1 TeV this was at 8.3° and for 3 Tev this was at 9.1°. In table 5.7 we show the median angular resolution after all the level 3 cuts and before the cone cut is made and the final effective volume after the cone cut.

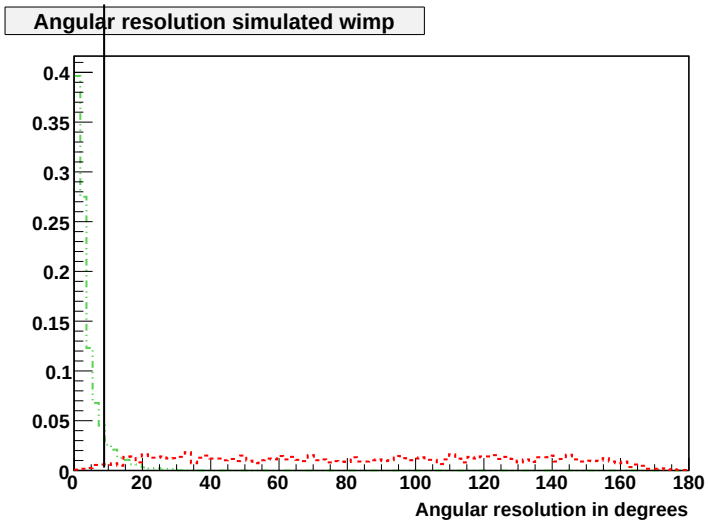

Figure 5.16: Normalized plot of the angle to the Sun for the simulated 1 TeV hard WIMP(green, dash-dotted) and the experimental data (red, dotted) that remains after the final cut. The black line shows the cut on the space angle for the 1TeV WIMP signal.

Table 5.7: The median angular resolution Ψ at final cut (before angular cut) and effective volume V_{eff} for WIMP signals in final sample after the resolution cut.

m_χ (TeV)	Channel	Ψ	V_{eff} km^3
1	hard	2.48°	$3.47 \cdot 10^{-2}$
3	soft	2.77°	$7.51 \cdot 10^{-3}$

5.6 Sensitivity of the detector and the anlysis.

Now because we did not construct our cone around the actual Sun position we should have a data sample that only contains background. From this sample we'll estimate the sensitivity of the Ic40 IceCube detector and the analysis presented in this thesis. Depending on the results of the experiment we would like to put the most restrictive limits on a theoretical signal or maximize the significance of the observation.[49, 50] We can't decide which one to use by looking at the experimental data in the actual cone around the Sun because this would lead to confidence intervals that do not have frequentist coverage. In order to estimate the sensitivity we use the average

upper limit. To calculate the average upper limit for the expected amount of background events n_b derived from the data sample we calculate the sum of the Feldman Cousins 90% confidence upper limit for each value of observed number events weighted with the poisson probabilility of occurrence

$$\overline{\mu}_s^{90\%}(n_b) = \sum_{n_{obs}}^{\infty} \mu_s^{90\%}(n_{obs} n_b) \frac{(n_b)^{n_{obs}}}{n_{obs}} e^{-n_b} \tag{5.10}$$

The physical quantity that neutrino telescopes measure directly is the neutrino-to-muon conversion rate $\Gamma_{\nu\to\mu}$, the upper limit on this is given by the formula

$$\Gamma_{\nu\to\mu} = \frac{\overline{\mu}_s^{90\%}}{V_{eff} \cdot t_{lifetime}} \tag{5.11}$$

For the 1 TeV hard 36 events where left for the 3 Tev soft 40 events where left.

For the neutralino dark matter model the annihilation rate can be calculate from $\Gamma_{\nu\to\mu}$. The annihilation rate to a given channel is directly proportional to the neutrino to muon conversion rate

$$\Gamma_{\nu\to\mu} = \frac{\Gamma_A \cdot n}{4\pi D^2} \int_0^{\infty} dE_{\nu_\mu} \sigma_{\nu_\mu} \frac{dN_{\nu_\mu}^{ch}}{dE_{\nu_\mu}} \tag{5.12}$$

where D is the distance from the detector to the center of the Sun, n is the target number density and σ_{ν_μ} is neutrino-muon cross section.[40]

The muon flux can be calculated using the annihilation rate with the formula

$$\Phi_\mu(E_\mu \geq E_{thr}) = \frac{\Gamma_A}{4\pi D^2} \int_{E_{thr}}^{m_\chi} dE_\mu \frac{dN_\mu}{dE_\mu} \tag{5.13}$$

where E_{thr} is an energy threshold of a 1 GeV, $\frac{dN_\mu}{dE_\mu}$ includes the combined effect of neutrino production (SUSY model dependent), propagation, the interaction kinematics and subsequent muon energy losses. The muon flux is used most to compare between different experiments. The results of this analysis are shown in table 5.8.

Table 5.8: The average 90% CL upper limit on the number of signal events $\overline{\mu}_s^{90\%}$, the upper limit on the conversion rate $\Gamma_{\nu\to\mu}$, the upper limit on the annihilation rate in the Sun Γ_A and the muon flux Φ_μ.

m_{chi} (TeV)	Channel	$\overline{\mu}_s^{90\%}$	$\Gamma_{\nu\to\mu}$ $(km^{-3}y^{-1})$	Γ_A (s^{-1})	Φ_μ $(km^{-2}y^{-1})$
1	hard	11.6	$7.65 \cdot 10^3$	$1.36 \cdot 10^{22}$	$4.1 \cdot 10^3$
3	soft	12.1	$7.71 \cdot 10^4$	$3.88 \cdot 10^{23}$	$4.7 \cdot 10^3$

Chapter 6

Summary and conclusion

The purpose of this thesis was the search for a signal from the 1 TeV neutralino annihilating with a hard neutrino spectrum (W^+W^-) and the 3 TeV neutralino annihilating with a soft neutrino spectrum, using 17 days of data taken with the IC40 IceCube detector in the year 2008. These particles are dark matter candidates, a hypothesised yet unseen form of matter which permeates our universe according to the current standard model of cosmology. The first objective of the analysis is to separate the neutrino signal from the atmospheric background, using Monte Carlo simulations of the background and of the two neutralino signals. Then an angular cone is created around the Sun to select WIMP like events. Because of unblinding requirements we don't set the cone around the Sun but instead place the cone away from the Sun selecting background events only. With this we determine the sensitvity of the IceCube detector, our main results are shown in table 5.7 and 5.8. We determine the effective volume V_{eff} from the Monte Carlo simulation as a measurement of the efficiency of the detector. From the experimental data in the cone we determine 90% upper limits on the number of signal events $\overline{\mu}_s^{90\%}$, on the conversion rate $\Gamma_{\nu\to\mu}$, on the annihilation rate in the Sun Γ_A and on the muon flux Φ_μ.The muon flux can be compared with the results from other experiments and the expected sensitivity for the complete IceCube detector 6.1 and 6.1.

A first step in improving this annalysis would be to determine the systematic errors on the effective volume V_{eff}. These systematic uncertainties are expected to be of the order of 20% to 30%.

The results this thesis can be compared with those in the IC22 dark matter analysis [48], which uses 104 days of data and adds an extra step to the analysis by making multi dimensional seection with Support Vector Machines.

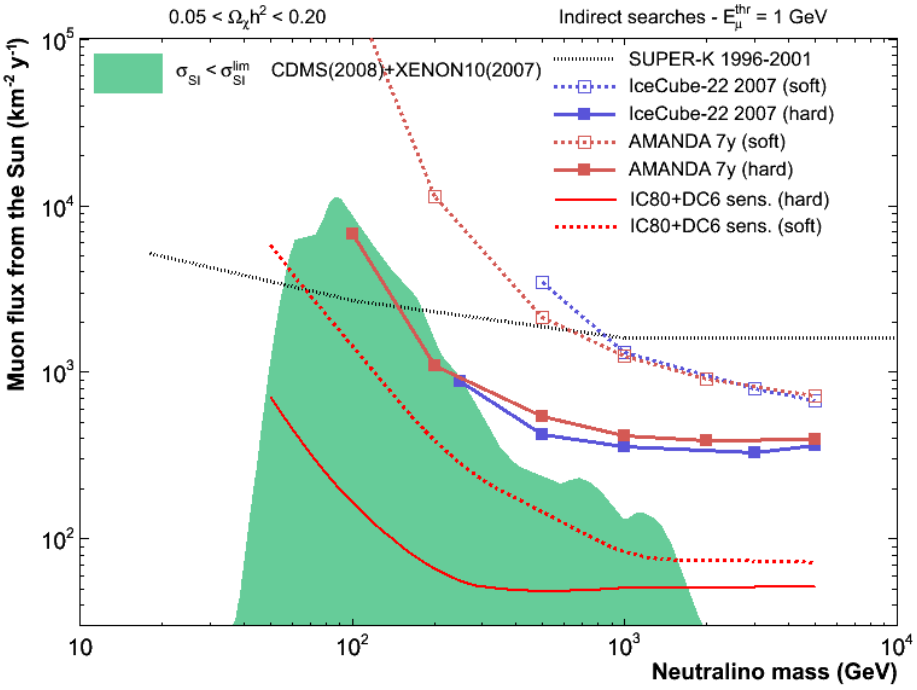

Figure 6.1: The plot shows the upperlimits on the muon flux for different experiments as function of the neutralino mass. The shaded aea shows predicted values of MSSM which are not excluded by experiment (direct searches and collider experiments)

These results are about an order of 10 better becouse more statistics was used but with only about half the detector. From this we conclude that multidimensional methods are a powerful tool to distinguish signal from background in IceCube dark matter searches.

The IceCube detector will also be completed in 2011. Using the full IceCube detector for data taking will should increase the sensitivty quite strongly especially for lower energes with the inclusion of Deep Core.

Table 6.1: The average 90% CL upper limit on the number of signal events $\overline{\mu}_s^{90\%}$, the upper limit on the conversion rate $\Gamma_{\nu\to\mu}$, the upper limit on the annihilation rate in the Sun Γ_A and the muon flux Φ_μ. Taken from the IC22 dark matter analysis.

m_{chi} (TeV)	Channel	Sensitivity $\overline{\mu}_s^{90\%}$	$\Gamma_{\nu\to\mu}$ $(km^{-3}y^{-1})$	Γ_A (s^{-1})	Φ_μ $(km^{-2}y^{-1})$
1	hard	12.0	$5.2 \cdot 10^2$	$9.1 \cdot 10^{20}$	$2.7 \cdot 10^2$
3	soft	13.0	$2.7 \cdot 10^3$	$8.5 \cdot 10^{21}$	$6.1 \cdot 10^2$

Bibliography

[1] Donald Perkins, *Particle Astrophysics second edition*,Oxford University Press (2009)

[2] Zwicky, F. (1937). *On the Masses of Nebulae and of Clusters of Nebulae*. Astrophysical Journal 86: 217.

[3] V. Rubin, W. K. Ford, Jr (1970). *Rotation of the Andromeda Nebula from a Spectroscopic Survey of Emission Regions*. Astrophysical Journal 159: 379.

[4] Taylor, A. N., Dye, S., Broadhurst, T. J., Benitez, N. and van Kampen, E. (jul 1998). *Gravitational Lens Magnification and the Mass of Abell 1689*. The Astrophysical Journal 501: 539. arXiv:astro-ph/9801158.

[5] N. Scoville, H. Aussel, A. Benson, A. Blain et al, *Large Structures and Galaxy Evolution in COSMOS at $z \leq 1.1$*, arXiv:astro-ph/0612384v1

[6] M. Carroll, *An introduction to General Relativity spacetime and Geometry*,Benjamin Cummings 2004

[7] The hubble website http://hubblesite.org/

[8] The NASA website http://www.nasa.gov/

[9] Springel, V. et al. (jun 2005). *Simulations of the formation, evolution and clustering of galaxies and quasars*,Nature 435:629-636,2005 , arXiv:astro-ph/0504097.

[10] W. Christoffel, *Introduction to cosmology* VUB course 2009

[11] Ying-Qiu Gu (May 2009), *Stationary Spiral Structure and Collective Motion of the Stars in a Spiral Galaxy*, arXiv:0805.2828v3

[12] Milgrom, M. (1983), *A modification of the Newtonian dynamics - Implications for galaxies*, Astrophysical Journal 270: 371389

[13] Randall et al, *Constraints on the Self-Interaction Cross-Section of Dark Matter from Numerical Simulations of the Merging Galaxy Cluster*, arXiv:0704.0261v1

[14] Gianfranco Bertone, Dan Hooper, Joseph Silk, *Particle Dark Matter: Evidence, Candidates and Constraints*, Phys.Rept.405:279-390,2005, arXiv:hep-ph/0404175v2

[15] R. D. Peccei, H. R. Quinn (1977). *CP Conservation in the Presence of Pseudoparticles*. Physical Review Letters 38: 1440. doi:10.1103/PhysRevLett.38.1440.

[16] Raffelt, G. (1995), *AXIONS IN ASTROPHYSICS AND COSMOLOGY*, arXiv:hep-ph/9502358

[17] Stephen P. Martin (2008), *A Supersymmetry Primer*, arXiv:hep-ph/9709356

[18] Francis Halzena, Dan Hooper *The Indirect Search for Dark Matter with IceCube*,New J.Phys.11:105019,2009, arXiv:0910.4513v2

[19] The CDMS website http://cdms.berkeley.edu/

[20] The XENON website http://xenon.physics.rice.edu/xenon100.html

[21] R. Barnabei et al. (2008). *First results from DAMA/LIBRA and the combined results with DAMA/Na*, Eur.Phys.J.C56:333-355,2008, arXiv:0804.2741

[22] F. Montanet, *Design and expected performance of the ANTARES neutrino telescope*,Nucl.Phys.Proc.Suppl. 87 (2000) 436-438,arXiv:astro-ph/0001380

[23] The CERN website http://public.web.cern.ch/public/

[24] Z. Ahmed, et al, *Results from the Final Exposure of the CDMS II Experiment*, arXiv:0912.3592

[25] J.L. Feng (2009). *Testing the Dark Matter Interpretation of the DAMA/LIBRA Result with Super-Kamiokande*, JCAP 0901:032,2009, arXiv:0808.4151v3

[26] The IceCube website http://icecube.wisc.edu/

[27] R. Roosen, College nota's 2009 ,*Fenomenologie van de elektromagnetische- Sterke- en zwakke wisselwerkingen*

[28] J.G. Learned and K.Mannheim, *Ann Rev. of Nucl.* Sc. 50 (2000) 679

[29] W.D. Leo, *Techniques for Nuclear and Particle Physics Experiments* ,Springer, (1994)

[30] I. Frank and I. Tamm, *Coherent radiation of fast electrons in a medium*, C. R. Ac. Sci. U.S.S.R. 14 (1937) 107.

[31] The Particle Data Group, http://pdg.lbl.gov/ (2010)

[32] AMANDA Collaboration, M. Ackermann et al., *Optical properties of deep glacial ice at the South Pole*, J. Geophys. Res. 111 (2006) D13203.

[33] Abbasi, R et al, *The IceCube Data Acquisition System: Signal Capture,3 Digitization, and Timestamping*,Nuclear Instruments and Methods A 601: 294316. doi:10.1016/j.nima.2009.01.001.

[34] D. Heck et al, *Extensive Air Shower Simulations with CORSIKA and the Influence of High-Energy Hadronic Interaction Models*, arXiv/0103073v1

[35] S. Ostapchenko,*Status of QGSJET*, arXiv:0706.3784.

[36] http://dima.lbl.gov/d̃ima/work/CORSIKA/(2010)

[37] A. Gazizov and M. O. Kowalski, *ANIS: High energy neutrino generator for neutrino telescopes*, Comp. Phys. Comm. 172 (2005) 203, astro-ph/0406439.

[38] H. Lai, J. Huston, S. Kuhlmann, J. Morfin, F. Olness, J. Owens, J. Pumplin, and W. Tung, *Global QCD analysis of parton structure of the nucleon: CTEQ-5 parton distributions*, Eur. Phys. J. C12 (2000) 375, hep-ph/9903282

[39] M. Blennow, J. Edsj and T. Ohlsson, *Neutrinos from WIMP Annihilations Obtained Using a Full Three-Flavor Monte Carlo Approach*,JCAP 0801:021,2008 , arXiv:0709.3898

[40] P.Gondolo et al., *JCAP* 0407 (2004) 08

[41] T.Sjöstrand et al., *JHEP* 05 (2006) 026

[42] Dmitry Chirkin, Wolfgang Rhode, *Propagating leptons through matter with Muon Monte Carlo (MMC)*, hep-ph/0407075

[43] J. Lundberg et al., *Light tracking through ice and water – Scattering and absorption in heterogeneous media with Photonics*, Nucl.Instrum.Meth.A581:619-631,2007 , astro-ph/0702108.

[44] Dmitry Chirkin, *Feature Extraction of IceCubeWaveforms*

[45] The AMANDA Collaboration, *Muon Track Reconstruction and Data Selection Techniques in AMANDA*, Nucl.Instrum.Meth.A524:169-194,2004, arXiv:astro-ph/0407044v1

[46] A. Rizzo, *GenN++: Generator of neutrino-nucleon interactions. Vrije Universiteit Brussel*, March 2006.

[47] D. Hubert, *Search with the AMANDA detector for neutralino dark matter in the Sun*, ph D thesis May 2009

[48] G. Wikström, *A Search for Solar Dark Matter with the IceCube Neutrino Telescope*, ph D thesis October 2009.

[49] G.J. Feldman and R.D. Cousins, *Unified approach to the classical statisctcal analysis of small signals*, Phys. Rev. D57 3873 (1998)

[50] G. Hill and K. Rawlins, *Unbiased cut selection for optimal upper limits in neutrino detectors: the model rejection potential technique*, Astropart.Phys. 19 (2003) 393-402